Development and in vitro evaluation of new bifunctional 89Zr-chelators based on the 6-amino-1,4-diazepane scaffold for immuno-PET applications

Benedikt Klasen, Daniel Lemcke, Thomas L Mindt, Gilles Gasser, Frank Rösch

Development and *in vitro* evaluation of new bifunctional ^{89}Zr-chelators based on the 6-amino-1,4-diazepane scaffold for immuno-PET applications

Benedikt Klasen[1], Daniel Lemcke[1], Thomas L. Mindt[2,3], Gilles Gasser[4], Frank Rösch[1]

[1]Department of Chemistry – TRIGA site, Johannes Gutenberg University Mainz, Germany

[2]Ludwig Boltzmann Institute Applied Diagnostics, General Hospital Vienna, Austria

[3]Department of Inorganic Chemistry, Faculty of Chemistry, University of Vienna, Austria

[4]Chimie ParisTech, PSL University, CNRS, Institute of Chemistry for Life and Health Sciences, Laboratory for Inorganic Chemical Biology, Paris, France

First author: Benedikt Klasen, phone: +49-6131-39-28498, email: b.klasen@uni-mainz.de

Corresponding author: Frank Rösch, Department of Chemistry – TRIGA site, Johannes Gutenberg University, Fritz-Strassmann Weg 2, D-55128 Mainz, Germany; phone: +49-6131-39-25302, fax: +49-6131-39-24692, email: frank.roesch@uni-mainz.de

Abbreviated title

New ^{89}Zr-chelator based on 6-amino-1,4-diazepane

Keywords

Zirconium-89, Hybrid-chelator, Hydroxamic acid, Deferoxamine, Antibody, Immuno-PET

Abstract

Introduction: Combination of hydroxamate bearing side chains with the 6-amino-1,4-diazepane scaffold provides a promising strategy for fast and stable ^{89}Zr-labeling of antibodies. Following this approach, we hereby present the development, labeling kinetics and *in vitro* complex stability of three resulting bifunctional chelator derivatives both stand-alone and coupled to a model protein in comparison to different linear deferoxamine (DFO) derivatives.

Methods: The novel ^{89}Zr-chelator Hy_3ADA^5 was prepared via amide-coupling of separately synthesized 6-amino-1,4-diazepane-6-pentanoic acid and hydroxamate-containing side chains. Two further bifunctional derivatives were synthesized by extending the resulting system with either a squaramide or *p*-isothiocyanatophenyl moiety for simplified binding to proteins. After coupling to a model antibody and purification, the resulting immunoconjugates as well as the unbound chelator derivatives were ^{89}Zr-labeled at room temperature (RT) and neutral pH. For comparison, different DFO derivatives were analogously coupled, purified and radiolabeled. *In vitro* complex stability of the resulting radioconjugates was investigated in phosphate buffered saline (PBS) and human serum at 37 °C over a period of 7 days.

Results: ^{89}Zr-labeling of the novel unbound Hy_3ADA^5 derivatives indicated rapid complexation kinetics resulting in high radiochemical conversions (RCC) of 84–94 % after 90 min. Similar or even faster radiolabeling with slightly increased maximum yields was obtained using the DFO-analogues. Initially, [^{89}Zr]Zr-DFO*-*p*-Ph-NCS showed a delayed formation, nevertheless reaching almost quantitative complexation. Radiolabeling of the corresponding immunoconjugates Hy_3ADA^5-SA-mAb and Hy_3ADA^5-*p*-Ph-NCS-mAb resulted in 82.0 ± 1.1 and 89.2 ± 0.7 % RCC, respectively after 90 min representing high but slightly lower labeling efficiency compared to the DFO- and DFO*-functionalized analogues. All examined radioimmunoconjugates showed very high *in vitro* complex stability both in human serum and PBS, providing no significant release of the radiometal. In the case of unbound chelators, however,

the *p*-Ph-NCS-functionalized derivatives indicated considerable instability in human serum already after one hour.

Conclusion: The novel chelator derivatives based on hydroxamate-functionalized 6-amino-1,4-diazepane revealed fast and high yielding ^{89}Zr-labeling kinetics as well as high *in vitro* complex stability both stand-alone and coupled to an antibody. Therefore, Hy_3ADA^5 represents a promising tool for radiolabeling of biomolecules such as antibodies at mild conditions for immuno-PET applications.

1. Background

In the past years, utilization of monoclonal antibodies (mAbs) for imaging of cancer and other diseases via immuno-positron emission tomography (immuno-PET) has gained increasing importance. Due to their highly selective binding to specific targets, antibodies being labeled with a positron-emitting radionuclide represent excellent tools not only for initial diagnosis but also for drug development, individual treatment planning, patient selection and monitoring of therapeutic progresses. [1–6].

The physical half-life represents a crucial factor in the selection of a suitable radionuclide for immuno-PET applications, since it has to match the typically slow pharmacokinetics of intact antibodies to ensure an optimal contrast defined by high target accumulation versus low residual activity circulating in the blood and non-target tissues [1,2,5–9]. Among several other longer-lived positron emitters, the radiometal zirconium-89 provides excellent and advantageous properties. Its physical decay half-life of 78.4 h matches almost exactly the biological half-life of full-size antibodies and therefore allows for high-quality PET-imaging even several days post administration of the corresponding radioconjugate, i.e. within a period that is typically required for optimal target-to-background ratios [6,8]. Additionally, due to low maximum and average positron energies of 902 keV and 396 keV, respectively, the mean range of the emitted particles (in water) is merely 1.23 mm prior to annihilation thus leading to a high spatial resolution [9–12]. Zirconium-89 decays via β^+ (22.8 %) and electron capture (76.2 %) to the metastable yttrium-89m, which in turn is transformed into the stable yttrium-89 by γ-deexcitation [12].

This almost exclusively (99.9 %) occurring γ-emission of 909 keV is outside the detection range of the PET-relevant 511 keV photons (350–650 keV), and thus does not cause any interfering incidents [1,9,13,14]. Zirconium-89 therefore gained extensively increased interest for immuno-PET applications in recent years.

The gold standard and to date almost exclusively used chelator for complexation of zirconium-89 is deferoxamine (DFO) [2,6,7,9,13]. The bacteria-produced siderophore DFO-B contains three hydroxamate groups and a terminal primary amine leading to an open-chain hexadentate bifunctional structure. Among multiple different approaches for stable coupling of the chelator to the protein, utilization of a *p*-isothiocyanatophenyl-functionalized DFO derivative, which provides a single step linkage to the lysine side chains of the antibody via formation of a stable thiourea bond, quickly became the method of choice for ^{89}Zr-labeling of monoclonal antibodies [15].

Since tetravalent oxophilic Zr^{4+} offers eight coordination sites and therefore prefers an octadentate coordination geometry, the six donor oxygens of DFO are supplemented by two additional water molecules in aqueous solution, resulting in a $[^{89}Zr][Zr(DFO)\text{-}cis\text{-}(H_2O)_2]^+$ complex tending to be sensitive to deprotonation [16–18]. Reportedly, DFO-functionalized, ^{89}Zr-labeled proteins therefore frequently show a certain (metabolic) instability *in vivo* leading to a release of the osteophilic radiometal and undesired accumulation in bone tissue [19–22]. Therefore, in recent years, several approaches have been pursued to develop new linear or macrocyclic chelator derivatives aiming for an improved complex stability based on more rigid systems or an increased number of donor atoms [6,7]. Among others, these include modified or extended versions of deferoxamine like DFO*, DFO-squaramide, DFO-cyclo* and oxoDFO* as well as other hydroxamate-based systems like fusarinin-C and respectively functionalized cyclen and cyclam derivatives [23–32]. Furthermore, hydroxypyridinone-systems like HOPO, 2,3-HOPO and CP256 or terephthalamide-containing structures such as TAM1 and TAM2 were introduced [33–36].

Two further chelator systems that have shown very promising results in combination with various radiometals such as gallium-68, scandium-44, copper-64 and lutetium-177 are AAZTA (1,4-Bis(carboxymethyl)-6-[bis(carboxymethyl)]amino-6-methylperhydro-1,4-diazepine) and DATA^{m} (1,4-Bis(carboxymethyl)-6-[(carboxymethyl)methylamino]-6-methylperhydro-1,4-diazepine) as well as the corresponding bifunctional derivatives AAZTA^{5} and DATA^{5m}. Both are based on a backbone consisting of two nitrogens being part of a macrocyclic diazepane scaffold and one exocyclic nitrogen. These hybrid chelator structures therefore combine the advantages of both linear and cyclic systems enabling fast radiolabeling at mild conditions as well as high complex stability [37–49]. However, in our preliminary experiments squaramide-functionalized AAZTA^{5} did not show any complexation of ^{89}Zr, at least at room temperature and neutral pH (data not shown).

Fig. 1

Therefore, we hereby present the development and *in vitro* evaluation of novel ^{89}Zr-chelator derivatives based on hydroxamate-functionalized 6-amino-1,4-diazepane for future immuno-PET applications. Compared to linear DFO derivatives, the more rigid basic scaffold in combination with six oxygen donors being potentially supported by three additional amide groups represents a promising system to ensure high ^{89}Zr-complex stability while still allowing for rapid radiolabeling kinetics under mild conditions. Analogously to AAZTA^{5} and DATA^{5m}, bifunctionality is given by means of a pentanoic acid linker (Fig. 1). Two further bifunctional derivatives were prepared by extending the free carboxylic acid with either a *p*-isothiocyanatophenyl or squaramide functionality for bioconjugation chemistry. Similarly to the thiourea-strategy, utilization of a squaramide linker provides straightforward functionalization of amine residues of the antibody selectively leading to squaric acid diamides. Despite several beneficial advantages such as high selectivity for primary amines, stepwise pH dependent amidation and introduction of further potential donor oxygens, squaramide-coupling still represents an unconventional but innovative method in radiopharmaceutical chemistry [50,51].

We evaluated these novel bifunctional chelator derivatives regarding ^{89}Zr-labeling kinetics at mild conditions and *in vitro* complex stability both stand-alone and coupled to the antibody bevacizumab (trade name Avastin®). In our study, this commercially available VEGF-A inhibitor merely served as model biomolecule with mAb profile without addressing its pharmacology in detail. For comparison, we analogously investigated different DFO derivatives and their corresponding immunoconjugates (Fig. 2).

Fig. 2

2. Materials and Methods

2.1 General

All nonradioactive chemicals were purchased from Sigma-Aldrich, Merck, VWR, TCI, Acros Organics, Fluka, AlfaAesar, Fisher Scientific, Chematech and Macrocyclics and used without further purification unless otherwise declared. For radiolabeling reactions trace metal-free substances were used. Column chromatography was performed using silica gel 60 (0.063–0.200 mm, Acros Organics) as stationary phase and the respectively specified solvents as mobile phase. NMR measurements were performed using a Bruker Avance III HD 400 (400 MHz) or Avance III 600 (600 MHz). ESI^+ mass spectrometry was measured via Agilent Technologies 1220 Infinity LC system coupled to an Agilent Technologies 6130 Single Quadrupole LC/MS system. HPLC purification and analysis was performed using a Merck LaChrom system with Hitachi L7100 pump and L7400 UV-detector and the respectively mentioned column and conditions. Purification of the immunoconjugates was performed via fractionated SEC using PD-10 Desalting Columns (8.3 mL Sephadex™ G-25, GE Healthcare). Matrix-assisted laser desorption/ionization (MALDI) mass spectrometry was measured in linear positive mode via Bruker autoflex® maX MALDI-TOF/TOF system and analyzed via Bruker flexAnalysis software. For radiolabeling experiments n.c.a. [^{89}Zr]Zr-oxalate in 1 M oxalic acid (PerkinElmer, Boston, USA) was used. Radioactivity of the samples was measured using a PC-based dose calibrator (ISOMED 2010, Nuklear Medizintechnik Dresden GmbH). Radiochemical conversions and purities were determined via radio

thin layer chromatography (radio-TLC, stationary phase: Merck Silica 60 F_{254} TLC plates; mobile phase: 0.1 M citrate-buffer pH 4), image plate scanner (CR35-Bio, Elysia Raytest) and AIDA Image Analysis software (Elysia Raytest).

2.2 Organic Synthesis

4-((Benzyloxy)(methyl)amino)-4-oxobutanoic acid (**4**)

4-((Benzyloxy)(methyl)amino)-4-oxobutanoic acid **4** was synthesized in four steps according to the literature [52]. Detailed synthesis descriptions are provided in the Supporting Information.

Methyl-5-(1,4-dibenzyl-6-nitro-1,4-diazepan-6-yl)pentanoate (**5**)

A mixture of 2-nitrocyclohexanone (2.00 g, 13.9 mmol), Amberlyst® A21 (1.05 g) and abs. methanol (35 mL) was stirred at 60 °C under reflux for 1 h. *N*,*N'*-Dibenzylethylenediamine (3.36 g, 13.9 mmol) and paraformaldehyde (1.67 g, 55.5 mmol) were added to the solution. The resulting suspension was heated to 80 °C and stirred overnight. After completion of the reaction, the mixture was filtered and the filtrate was evaporated under reduced pressure. After purification via column chromatography (cyclohexane/ethylacetate 9:1, R_f = 0.27) product **5** was obtained as yellow oil (5.20 g, 11.8 mmol, 85 %). ^{1}H-NMR ($CDCl_3$, 400 MHz, δ [ppm]): 7.27 (m, 10 H); 3.72 (d, J = 13.1 Hz, 2 H); 3.64 (s, 3 H); 3.56 (d, J = 13.0 Hz, 2 H); 3.49 (d, J = 14.2 Hz, 2 H); 2.94 (d, J = 14.2 Hz, 2 H); 2.59 (m, 4 H); 2.09 (t, J = 7.6 Hz, 2 H); 1.55 (m, 2 H); 1.29 (m, 2 H); 0.76 (m, 2 H). ^{13}C-NMR ($CDCl_3$, 100 MHz, δ [ppm]): 173.6 (s); 139.1 (s); 129.1 (s); 128.3 (s); 127.3 (s); 94.8 (s); 64.9 (s); 61.8 (s); 58.9 (s); 51.5 (s); 36.5 (s); 33.6 (s); 24.6 (s); 22.6 (s). MS ESI$^+$ (m/z): found 440.3 [M+H$^+$], calculated for $C_{25}H_{33}N_3O_4$: 439.25.

Methyl-5-(6-(4-((benzyloxy)(methyl)amino)-4-oxobutanamido)-1,4-bis(4-((benzyloxy)(methyl)amino)-4-oxobutanoyl)-1,4-diazepan-6-yl)pentanoate (**7**)

5 (505 mg, 1.15 mmol) was dissolved in abs. methanol (15 mL) and a catalytic amount of $Pd(OH)_2/C$ (20 wt%) was added. The resulting mixture was stirred intensively for 16 h under an atmosphere of hydrogen. After completion of the reaction, the catalyst was removed via filtration over Celite® and the filtrate was evaporated under reduced pressure. The crude yellowish, oily product **6** (246 mg) was used for the following reaction without further purification. MS ESI^+ (m/z): found 230.2 $[M+H^+]$, calculated for $C_{11}H_{23}N_3O_2$: 229.18.

To a solution of **4** (914 mg, 3.85 mmol) and DIPEA (2.01 mL, 11.8 mmol) in anhydrous DMF (15 mL) HATU (1.88 g, 4.94 mmol) was added and the resulting mixture was stirred for 1 h at room temperature under argon atmosphere. Subsequently **6** (246 mg, 1.07 mmol) was added and stirring continued overnight. After evaporation of the solvent under reduced pressure, the residue was dissolved in chloroform (30 mL), washed with water (3 x 10 mL), dried over Na_2SO_4 and evaporated again. The crude product was purified via column chromatography (chloroform/methanol 25:1, R_f = 0.36) to yield **7** (487 mg, 0.55 mmol, 51 %) as amber-colored solid. ^{1}H-NMR ($CDCl_3$, 400 MHz, δ [ppm]): 7.44–7.31 (m, 15 H); 4.96–4.80 (m, 6 H); 4.51 (dd, J = 15.0, 7.8 Hz, 1 H); 4.08–3.97 (m, 1 H); 3.72–3.59 (m, 3 H); 3.49–3.38 (m, 1 H); 3.37–3.24 (m, 2 H); 3.22 (s, 1 H); 3.19–3.16 (m, 3 H); 3.13 (d; J = 5.46, 4 H); 3.01–2.86 (m, 2 H); 2.83 (s, 3 H); 2.80–2.47 (m, 10 H); 2.46–2.34 (m, 2 H); 2.34–2.23 (m, 2 H); 1.66–1.54 (m, 2 H); 1.44–1.19 (m, 3 H). MS ESI^+ (m/z): found 887.4 $[M+H^+]$, calculated for $C_{47}H_{62}N_6O_{11}$: 886.45.

5-(6-(4-((Benzyloxy)(methyl)amino)-4-oxobutanamido)-1,4-bis(4-((benzyloxy)(methyl)amino)-4-oxobutanoyl)-1,4-diazepan-6-yl)pentanoic acid (**8**)

1 M LiOH (508 µL, 0.51 mmol) was added to a solution of **7** (226 mg, 0.25 mmol) in 1,4-dioxane/water (2:1, 3 mL) and the resulting solution was stirred for 3 h at room temperature. After evaporation of the solvents under reduced pressure, the residue was treated with 1 M $NaHCO_3$ (10 mL) and extracted with chloroform (4 x 10 mL). The combined organic extracts were dried over Na_2SO_4 and evaporated under reduced pressure yielding **8** (171 mg, 0.20 mmol, 78 %) as colorless solid. ^{1}H-NMR ($CDCl_3$,

400 MHz, δ [ppm]): 7.42–7.27 (m, 15 H); 4.92–4.79 (m, 5 H); 4.55–4.36 (m, 2 H); 4.32–4.11 (m, 2 H); 4.10–3.88 (m, 2 H); 3.36–3.07 (m, 10 H); 2.96–2.81 (m, 3 H); 2.80 (s, 3 H); 2.78–2.24 (m, 11 H); 2.23–2.09 (m, 2 H); 1.61–1.44 (m, 2 H); 1.42–1.17 (m, 3 H). ^{13}C-NMR ($CDCl_3$, 100 MHz, δ [ppm]): 180.0 (s); 175.3 (s); 174.0 (s); 172.9 (s); 172.6 (s); 134.8 (s); 134.6 (s); 129.3 (s); 129.3 (s); 129.2 (s); 129.2 (s); 128.9 (s); 128.7 (s); 128.7 (s); 128.6 (s); 128.4 (s); 128.3 (s); 127.8 (s); 77.25 (s); 76.2 (s); 75.6 (s); 67.1 (s); 61.4 (s); 56.0 (s); 50.4 (s); 49.9 (s); 47.0 (s); 46.8 (s); 39.3 (s); 38.6 (s); 36.5 (s); 36.4 (s); 33.4 (s); 31.4 (s); 31.1 (s); 27.9 (s); 27.5 (s); 26.9 (s); 25.9 (s); 22.9 (s). MS ESI$^+$ (m/z): found 873.4 [M+H$^+$], calculated for $C_{46}H_{60}N_6O_{11}$: 872.43.

5-(6-(4-(Hydroxy(methyl)amino)-4-oxobutanamido)-1,4-bis(4-(hydroxy(methyl)amino)-4-oxobutanoyl)-1,4-diazepan-6-yl)pentanoic acid (**9**)

To a solution of **8** (50 mg, 57.3 µmol) in abs. methanol (3 mL) a catalytic amount of Pd/C (10 wt%) was added. The resulting mixture was intensively stirred for 30 min under an atmosphere of hydrogen. After completion of the reaction the suspension was filtered over Celite® and the filtrate was evaporated under reduced pressure. After purification via HPLC (column: Phenomenex Synergi C18 semipreparative (250 x 10 mm) 4 µ, flow rate: 5 mL/min, 10 % to 16 % MeCN + 0.1 % TFA in 20 min, t_R = 14.8 min) **9** (9.1 mg, 15.1 µmol, 26 %) was obtained as pale amber-colored solid. MS ESI$^+$ (m/z): found 603.3 [M+H$^+$], calculated for $C_{25}H_{42}N_6O_{11}$: 602.29.

N^1-(6-(5-((2-(Benzylamino)ethyl)amino)-5-oxopentyl)-1,4-bis(4-((benzyloxy)(methyl)amino)-4-oxobutanoyl)-1,4-diazepan-6-yl)-N^4-(benzyloxy)-N^4-methylsuccinamide (**10**)

8 (171 mg, 0.20 mmol) was dissolved in anhydrous acetonitrile (3 mL) under argon atmosphere. Successively, HBTU (75 mg, 0.20 mmol), HOBt (78 mg, 0.58 mmol) and DIPEA (100 µL, 0.59 mmol) were added and the resulting mixture was stirred for 1 h at room temperature. *N*-Benzylethylenediamine (59 µL, 0.39 mmol) was added and stirring continued for further 3 h. After completion of the reaction,

the solvent was evaporated under reduced pressure and the residue was dissolved in chloroform (20 mL). The organic solution was washed with water (3 x 10 mL) and the aqueous phases were re-extracted once again with chloroform (20 mL). The combined organic extracts were dried over Na_2SO_4 and evaporated under reduced pressure yielding **10** (182 mg, 0.18 mmol, 92 %) as colorless oil. ^{1}H-NMR ($CDCl_3$, 400 MHz, δ [ppm]): 7.47–7.20 (m, 20 H); 4.96–4.79 (m, 5 H); 4.33–4.24 (m, 1 H); 4.07–3.99 (m, 2 H); 3.98–3.86 (m, 2 H); 3.70–3.60 (m, 2 H); 3.53–3.43 (m, 2 H); 3.31–3.22 (m, 1 H); 3.19–3.09 (m, 8 H); 3.07–2.92 (m, 2 H); 2.80 (s, 9 H); 2.75–2.61 (m, 4 H); 2.60–2.52 (m, 2 H); 2.44–2.38 (m, 1 H); 2.22–2.12 (m, 2 H); 1.49–1.10 (m, 6 H). MS ESI$^+$ (m/z): found 1005.5 [M+H$^+$], calculated for $C_{55}H_{72}N_8O_{10}$: 1004.54.

N^1-(6-(5-((2-Aminoethyl)amino)-5-oxopentyl)-1,4-bis(4-(hydroxy(methyl)amino)-4-oxobutanoyl)-1,4-diazepan-6-yl)-N^4-hydroxy-N^4-methylsuccinamide (**11**)

To a solution of **10** (100 mg, 99.5 µmol) in abs. methanol (5 mL) a catalytic amount of Pd/C (10 wt%) was added and the resulting mixture was intensively stirred for 4 h under an atmosphere of hydrogen. After completion of the reaction, the catalyst was removed via filtration over Celite® and the solvent was evaporated under reduced pressure to yield **11** (59.7 mg, 92.6 µmol, 93 %). ^{1}H-NMR ($CDCl_3$, 400 MHz, δ [ppm]): 3.72–3.63 (m, 4 H); 3.51–3.47 (m, 1 H); 3.28–3.17 (m, 5 H); 3.04–2.93 (m, 2 H); 2.83–2.77 (m, 2 H); 1.48–1.34 (m, 8 H); 1.31–1.17 (m, 7 H); 1.25 (s, 9 H); 1.16–1.09 (m, 2 H); 0.88 (t, J = 6.8 Hz, 2 H). MS ESI$^+$ (m/z): found 645.3 [M+H$^+$], calculated for $C_{27}H_{48}N_8O_{10}$: 644.35.

N^1-(6-(5-((2-((2-Ethoxy-3,4-dioxocyclobut-1-en-1-yl)amino)ethyl)amino)-5-oxopentyl)-1,4-bis(4-(hydroxy(methyl)amino)-4-oxobutanoyl)-1,4-diazepan-6-yl)-N^4-hydroxy-N^4-methylsuccinamide (**12**)

To a solution of **11** (17.8 mg, 27.6 µmol) in phosphate-buffer (0.5 M Na_2HPO_4/NaH_2PO_4, pH 7, 2 mL) 3,4-diethoxycyclobut-3-ene-1,2-dione (8.2 µL, 55.4 µmol) was added. The pH was readjusted to 7 with 1 M NaOH and the solution was stirred for 3 h at room temperature. After completion of the reaction,

the product was purified via HPLC (column: Phenomenex Synergi C18 semipreparative (250 x 10 mm) 4 µ, flow rate: 5 mL/min, 12 % to 18 % MeCN + 0.1 % TFA in 30 min, t_R = 18.0 min) yielding **12** (7.4 mg, 9.6 µmol, 35 %) as pale amber-colored solid. MS ESI$^+$ (m/z): found 769.4 [M+H$^+$], calculated for $C_{33}H_{52}N_8O_{13}$: 768.37.

N^1-(1,4-Bis(4-(hydroxy(methyl)amino)-4-oxobutanoyl)-6-(5-((2-(3-(4-isothiocyanatophenyl)thio-ureido)ethyl)amino)-5-oxopentyl)-1,4-diazepan-6-yl)-N^4-hydroxy-N^4-methylsuccinamide (**13**)

11 (20.0 mg, 31.0 µmol) was dissolved in isopropanol/water (4:1, 4 mL). Subsequently, a solution of 1,4-phenylene diisocyanate (61.2 mg, 0.32 mmol) in chloroform (4 mL) was added while stirring followed by immediate addition of triethylamine (40.5 µL, 0.29 mmol). The resulting mixture was stirred for 1 h at room temperature. After completion of the reaction the solvents were evaporated under reduced pressure and the crude product was purified via HPLC (column: Phenomenex Synergi C18 semipreparative (250 x 10 mm) 4 µ, flow rate: 5 mL/min, 25 % to 40 % MeCN + 0.1 % TFA in 20 min, t_R = 15.5 min) to yield **13** (7.3 mg, 8.7 µmol, 28 %) as colorless powder. MS ESI$^+$ (m/z): found 837.3 [M+H$^+$], calculated for $C_{35}H_{52}N_{10}O_{10}S_2$: 836.33.

Deferoxamine squaramide ethyl ester (**14**)

Deferoxamine squaramide ethyl ester **14** was synthesized according to the literature [25]. Detailed synthesis description is provided in the Supporting Information.

2.3 Antibody coupling and radiolabeling with ^{89}Zr

Synthesis and purification of Hy_3ADA^5-SA-mAb and DFO-SA-mAb

120 µL of bevacizumab solution (3.0 mg mAb, 20.1 nmol, 25 mg/mL, Avastin®, Roche) was diluted with 0.5 M Na_2HPO_4-buffer (pH = 9, 1 mL). A tenfold molar excess of a solution of either Hy_3ADA^5-SA (60.4 µL, 201.3 nmol, 2.563 mg/mL in DMSO) or DFO-SA (60.4 µL, 201.3 nmol, 2.283 mg/mL in DMSO) was added in 6 portions while shaking via thermomixer (500 rpm). The pH of the mixture was adjusted to 9 with 1 M NaOH solution before shaking overnight at room temperature. The resulting immunoconjugates were subsequently purified via fractionated SEC. In detail, the PD-10 column was first preconditioned with 20 mL PBS. The respective reaction mixture was then completely applied to the column and the flow-through was collected in the first fraction. Subsequently, a further 9 fractions of 0.5 mL PBS each were collected. The protein containing fractions 6 and 7 were combined and homogenized before subsequent radiolabeling.

Synthesis and purification of Hy_3ADA^5-p-Ph-NCS-mAb, DFO-p-Ph-NCS-mAb and DFO-p-Ph-NCS-mAb*

120 µL of bevacizumab solution (3.0 mg mAb, 20.1 nmol, 25 mg/mL, Avastin®, Roche) was diluted with 880 µL PBS and the pH of the mixture was adjusted to 9 with 0.1 M Na_2CO_3 solution. A tenfold molar excess of a solution of either Hy_3ADA^5-*p*-Ph-NCS (60.4 µL, 201.3 nmol, 2.790 mg/mL in DMSO), DFO-*p*-Ph-NCS (60.4 µL, 201.3 nmol, 2.510 mg/mL in DMSO) or DFO*-*p*-Ph-NCS (60.4 µL, 201.3 nmol, 3.177 mg/mL in DMSO) was added in 6 portions while shaking via thermomixer (500 rpm). The mixture was shaken for 1 h at 37 °C. The resulting immunoconjugates were subsequently purified via fractionated SEC similarly to the squaramide-coupled analogues.

Determination of chelator-to-antibody ratios (CAR) using MALDI-TOF mass spectrometry

Solutions of unmodified bevacizumab and of the SEC-purified immunoconjugates Hy_3ADA^5-SA-mAb, Hy_3ADA^5-*p*-Ph-NCS-mAb, DFO-SA-mAb, DFO-*p*-Ph-NCS-mAb and DFO*-*p*-Ph-NCS-mAb were desalted via PD-10 column and lyophilized. Subsequently, a 1:1 solution of acetonitrile and water containing 0.1 % TFA was added. The samples were mixed with a matrix solution of sinapinic acid on the target

plate, air dried and MALDI-TOF mass spectrometry was measured using linear positive mode. The obtained molecular weights were used to determine the average number of conjugated chelator moieties per protein as follows:

$$CAR = \frac{MW_{conj} - MW_{mAb}}{MW_{chel}}$$

with MW_{conj} = measured average molecular weight of the respective immunoconjugate, MW_{mAb} = measured average molecular weight of unmodified bevacizumab and MW_{chel} = mass gain per respectively conjugated chelator moiety.

Radiolabeling of Hy_3ADA^5, Hy_3ADA^5-SA, Hy_3ADA^5-p-Ph-NCS, DFO mesylate, DFO-SA, DFO-p-Ph-NCS and DFO-p-Ph-NCS with zirconium-89*

100 µL [^{89}Zr]Zr-oxalate solution (1 M oxalic acid, 10–12 MBq) was neutralized with 45 µL 2 M Na_2CO_3 solution and incubated for 3 min at room temperature. Subsequently, 150 µL 0.5 M HEPES-buffer (pH 7) and 200 µL of a solution of either Hy_3ADA^5, Hy_3ADA^5-SA, Hy_3ADA^5-*p*-Ph-NCS, DFO mesylate, DFO-SA, DFO-*p*-Ph-NCS or DFO*-*p*-Ph-NCS (20 nmol, 6 µL of 3.33 mmol/L chelator in DMSO diluted with 194 µL PBS) were added. Finally, the solution was filled up with further 255 µL 0.5 M HEPES-buffer (pH 7) to a total volume of 750 µL. The reaction mixture was shaken for 90 min at room temperature and 500 rpm via thermomixer. Radiolabeling efficiency was investigated at different times via radio TLC (^{89}Zr-labeled chelator: R_f = 0–0.1; free zirconium-89: R_f = 0.4–0.6).

Radiolabeling of Hy_3ADA^5-SA-mAb, Hy_3ADA^5-p-Ph-NCS-mAb, DFO-SA-mAb, DFO-p-Ph-NCS-mAb and DFO-p-Ph-NCS-mAb with zirconium-89 and purification of the resulting radioimmunoconjugates*

100 µL [^{89}Zr]Zr-oxalate solution (1 M oxalic acid, 10–12 MBq) was neutralized with 45 µL 2 M Na_2CO_3 solution and incubated for 3 min at room temperature. Subsequently, 150 µL 0.5 M HEPES-buffer (pH 7) and 200 µL of a PBS-solution of either Hy_3ADA^5-SA-mAb, Hy_3ADA^5-*p*-Ph-NCS-mAb, DFO-SA-mAb,

DFO-*p*-Ph-NCS-mAb or DFO*-*p*-Ph-NCS-mAb (472–731 µg protein) were added. Finally, the solution was filled up with further 255 µL 0.5 M HEPES-buffer (pH 7) to a total volume of 750 µL. The reaction mixture was shaken for 90 min at room temperature and 500 rpm via thermomixer. Radiolabeling efficiency was investigated at different times via radio TLC (^{89}Zr-labeled mAb: R_f = 0; free zirconium-89: R_f = 0.4–0.6). The resulting radioimmunoconjugates [^{89}Zr]Zr-Hy$_3$ADA^5-SA-mAb, [^{89}Zr]Zr-Hy$_3$ADA^5-*p*-Ph-NCS-mAb, [^{89}Zr]Zr-DFO-SA-mAb, [^{89}Zr]Zr-DFO-*p*-Ph-NCS-mAb and [^{89}Zr]Zr-DFO*-*p*-Ph-NCS-mAb were purified via fractionated SEC using the same conditions as for purification prior to radiolabeling. The antibody-containing fractions were identified by measurement of radioactivity and radiochemical purity was determined via radio-TLC before combination and homogenization.

2.4 Determination of *in vitro* complex stability of the ^{89}Zr-labeled chelator derivatives

The solution of [^{89}Zr]Zr-Hy$_3$ADA^5, [^{89}Zr]Zr-Hy$_3$ADA^5-SA, [^{89}Zr]Zr-Hy$_3$ADA^5-*p*-Ph-NCS, [^{89}Zr]Zr-DFO mesylate, [^{89}Zr]Zr-DFO-SA, [^{89}Zr]Zr-DFO-*p*-Ph-NCS or [^{89}Zr]Zr-DFO*-*p*-Ph-NCS (200 µL) was added to either 500 µL human serum or 500 µL PBS and the resulting mixtures were shaken via thermomixer at 37 °C and 500 rpm for 7 d. The proportion of the intact conjugate versus released radionuclide was determined via radio-TLC at various times.

2.5 Determination of *in vitro* complex stability of the ^{89}Zr-labeled radioimmunoconjugates

The purified radioimmunoconjugate [^{89}Zr]Zr-Hy$_3$ADA^5-SA-mAb, [^{89}Zr]Zr-Hy$_3$ADA^5-*p*-Ph-NCS-mAb, [^{89}Zr]Zr-DFO-SA-mAb, [^{89}Zr]Zr-DFO *p*-Ph-NCS-mAb or [^{89}Zr]Zr-DFO* *p*-Ph-NCS-mAb (in 300 µL PBS) was added to either 500 µL human serum or 500 µL PBS and the resulting mixtures were shaken via thermomixer at 37 °C and 500 rpm for 7 d. The proportion of the intact conjugate versus released radionuclide was determined via radio-TLC at various times.

3. Results and Discussion

3.1 Organic Synthesis

The benzyl-protected, hydroxamate bearing precursor **4** was synthesized in four steps with an overall yield of 87 % according to the procedure described by Olshvang *et al*. [52]. Starting from *O*-benzylhydroxylamine hydrochloride, successive Boc-protection, methylation, deprotection and reaction with succinic anhydride led to the desired product containing of a linkable carboxylic acid (Scheme 1).

The 6-amino-1,4-diazepane scaffold including a pentanoic acid linker was prepared similarly to the first steps of the AAZTA^5 synthesis already published by our group [43]. Formation of the diazepane cycle of **5** was achieved by *in situ* ring-opening of 2-nitrocyclohexane and subsequent double Nitro-Mannich reaction of the resulting nucleophilic compound with the iminium ion derived from *N,N'*-dibenzylethylenediamine and paraformaldehyde. Subsequently, catalytic hydrogenation led to simultaneous deprotection of the endocyclic amines and reduction of the nitro group to an exocyclic amine resulting in the desired precursor **6** (Scheme 1)**.**

Scheme 1

The next step first includes the combination of this hybrid structure with three hydroxamic acid bearing sidechains **4** via amidation using HATU as conventional coupling reagent. The remaining methyl ester of compound **7** was subsequently cleaved via base-catalyzed hydrolysis to provide the aforementioned pentanoic acid linker. Finally, hydrogenolytic deprotection of **8** and purification via HPLC led to the novel bifunctional chelator Hy_3ADA^5 (**9**, Scheme 1) with a yield of 9 % over all steps proceeding from *N*,*N'*-dibenzylethylenediamine.

Starting from the benzyl-protected structure **8**, a further synthesis route was pursued to produce two additional bifunctional derivatives of Hy_3ADA^5 that should simplify coupling chemistry in combination with amine bearing target vectors such as proteins. Therefore, mono-benzyl-protected ethylene

diamine was coupled to the free carboxylic acid via amidation to yield compound **10**. Subsequent hydrogenolytic deprotection of all four protecting groups resulted in derivative **11** providing a terminal primary amine, which in turn was reacted with squaric acid diethyl ester at pH 7 in the next step to finally obtain the squaramide-derivative Hy_3ADA^5-SA **12**. To prevent formation of the corresponding diamide at more basic conditions, accurate pH control using a suitable buffer medium is required. In a further approach, 1,4-phenylene diisocyanate was coupled to the primary amine of **11** via formation of a stable thiourea bond to yield Hy_3ADA^5-*p*-Ph-NCS **13**. In this case, formation of the chelator-dimer could also be completely avoided using a tenfold molar excess of diisocyanate linker and a two-phase solvent system. Both final structures Hy_3ADA^5-SA and Hy_3ADA^5-*p*-Ph-NCS were purified via HPLC before antibody coupling and radiolabeling experiments resulting in overall yields of 10 % and 8 %, respectively. The rather moderate yields of the final synthesis steps of **9**, **12**, and **13** do not reflect low formation of the end products (as confirmed via reaction control), but are more attributed to a loss in the course of HPLC purification.

In addition to the commercially available deferoxamine derivatives DFO mesylate, DFO-*p*-Ph-NCS and DFO*-*p*-Ph-NCS, the corresponding squaramide-analogue DFO-SA (**14**) was synthesized according to Rudd *et al.* starting from DFO mesylate and squaric acid diethyl ester [25]. After HPLC purification, the monoamide was obtained with a yield of 33 %.

3.2 Radiolabeling of the stand-alone chelator derivatives of Hy_3ADA^5 with zirconium-89 in comparison to corresponding deferoxamine systems

Prior to protein conjugation, the novel Hy_3ADA^5 and its derivatives Hy_3ADA^5-SA and Hy_3ADA^5-*p*-Ph-NCS were evaluated for their ^{89}Zr-labeling as stand-alone bifunctional chelators. Mild radiolabeling conditions were selected in accordance with conventional standard procedures for ^{89}Zr-labeling of deferoxamine-based radiotracers [53]. For comparison, DFO mesylate, DFO-SA, DFO-*p*-Ph-NCS and DFO*-*p*-Ph-NCS served as reference being investigated under identical conditions (Fig. 3, Table S1).

The hybrid systems based on 6-amino-1,4-diazepane generally indicated fast labeling kinetics leading to high radiochemical conversions. In detail, complexation of the radiometal via the basic structure Hy_3ADA^5 provided 67.7 ± 2.2 % bound activity already after 5 min and culminated in a maximum yield of 90.1 ± 1.6 % after 60 min. The squaramide-functionalized derivative Hy_3ADA^5-SA showed a slightly slower increase in bound activity, nevertheless reaching an even higher final radiochemical conversion of 93.6 ± 0.4 % after 90 min. Thus, the squaramide moiety spaced by six methylene groups and one amide bond obviously neither has a significant positive nor negative influence on the ^{89}Zr-labeling properties of the actual chelator system at least under the conditions used herein. The *p*-isothiocyanatophenyl-functionalized analogue Hy_3ADA^5-*p*-Ph-NCS revealed even slightly faster labeling kinetics compared to its parental system Hy_3ADA^5 (75.3 ± 12.1 % after 5 min) as well as final results similar to Hy_3ADA^5-SA (93.3 ± 0.2 % after 90 min).

Fig. 3

As expected, and confirming the typical behavior of linear, acyclic chelator systems, ^{89}Zr-labeling of DFO mesylate, DFO-SA and DFO-*p*-Ph-NCS provided even slightly faster complexation with radiochemical conversions of approx. 95–97 % already after 15 min without significant increase in the further course of the reaction. Apparently, both the squaramide and *p*-isothiocyanatophenyl moiety marginally affected the incorporation of the radiometal at the beginning of the reaction compared to non-functionalized deferoxamine but in the further progress almost identical radiochemical conversions were obtained. Formation of [^{89}Zr]Zr-DFO*-*p*-Ph-NCS indicated slightly delayed complexation of the tetravalent radiometal with 50.0 ± 8.6 % after 5 min, which is presumably due to an enhanced steric demand caused by the extended chain length of the actual chelator. Nevertheless, based on the higher quantity of hydroxamate donors, DFO*-*p*-Ph-NCS revealed excellent labeling properties with increasing duration up to almost quantitative conversion to the corresponding radioconjugate (98.9 ± 0.6 % after 90 min). In summary, the *p*-isothiocyanatophenyl-functionalized version showed the best results of newly developed Hy_3ADA^5 derivatives, whereas DFO mesylate and

DFO*-*p*-Ph-NCS indicated the fastest labeling kinetics and the highest overall yields, respectively of all herein studied chelators.

3.3 *In vitro* complex stability of the ^{89}Zr-labeled Hy_3ADA^5 and DFO derivatives

The ^{89}Zr-labeled bifunctional chelators were investigated regarding their *in vitro* complex stability both in phosphate buffered saline representing the later formulation medium and in human serum at 37 °C over a period of 7 days (Fig. 4, Table S2, S3). This time interval is adequate to account for both the half-life of zirconium-89 and the typical pharmacokinetics of full-size antibodies and thus covers an appropriate immuno-PET imaging period. After 7 days, the basic chelator scaffold Hy_3ADA^5 provided a percentage of bound radiometal of 89.7 ± 0.4 % and 89.7 ± 4.4 % in PBS and human serum, respectively, which even exceeded the initial purity of 84.4 %. In both media, small positive and negative fluctuations in the range between approx. 80 and 93 % were observed throughout the measurement period, presumably due to further complexation, minimal release and recomplexation of the radiometal. Starting from a radiochemical purity of 93.8 %, the squaramide-functionalized Hy_3ADA^5-SA revealed similarly high *in vitro* complex stability resulting in 95.5 ± 0.0 % and 90.9 ± 0.5 % after 7 days in PBS and human serum, respectively. While almost no release of free radiometal could be observed for [^{89}Zr]Zr-Hy_3ADA^5-*p*-Ph-NCS in formulation medium within 7 days, the radiocomplex disclosed considerable instability only after a short incubation time in human serum. After 24 h, only 30.5 ± 0.7 % bound activity, i.e. approx. 33 % of the initial value (93.3 %) was still present. Despite the fact that no further significant decrease was observed in the later course (31.1 ± 0.6 % after 7 days), this represents a major difference compared to the other two Hy_3ADA^5 derivatives. The free *p*-isothiocyanatophenyl linker therefore apparently affects the stability of the corresponding radiocomplex in combination with the components of human serum. Since isothiocyanates are also known to react under physiological conditions to form thiocarbamates, dithiocarbamates or thioureas, to some extent this effect is presumably related to the reaction of the free NCS-group with proteins or

smaller serum components such as free amino acids [54]. Instead of a distinct small spot representing free uncomplexed ^{89}Zr, in this case the radio-TLC results indicated a rather diffuse distribution of activity within a large range of approx. R_f = 0.4–1.0. Therefore, instability of the *p*-isothiocyanatophenyl-functionalized derivative may not or not only be based on a pure release of free radiometal, but also on alternatively occurring (decomposition) mechanisms leading to the formation of species with lower TLC-retention.

Fig. 4

In PBS, the analogously investigated DFO derivatives also revealed very high *in vitro* stability over the entire experimental period without any exception (Fig. 4A). As expressed by almost unchanged values of approx. 97–100 % intact conjugate, the ^{89}Zr-complexes of non-functionalized deferoxamine (mesylate), DFO-SA, DFO-*p*-Ph-NCS and DFO*-*p*-Ph-NCS indicated no measurable release of free radiometal within 7 days. In human serum, [^{89}Zr]Zr-DFO remained completely stable, whereas the squaramide-functionalized [^{89}Zr]Zr-DFO-SA initially showed the same behavior until day 3 before revealing a slight instability down to 93.8 ± 1.9 % incorporated activity within the following 4 days (Fig. 4B). Although this represents only a minor difference, improved stability due to the additional donor oxygens of the squaric acid moiety could therefore not be confirmed in this experiment, at least *in vitro*. Analogously to Hy_3ADA^5-*p*-Ph-NCS, both the *p*-isothiocyanatophenyl-derivatives of DFO and DFO* indicated a significant collapse of *in vitro* stability in human serum. While [^{89}Zr]Zr-DFO*-*p*-Ph-NCS still demonstrated 73.2 ± 1.6 % bound radiometal after 1 h, the corresponding value of the DFO-analogue dropped to only 34.5 ± 14.4 % within this short time. Both bifunctional chelator derivatives reached a minimum percentage of intact radioconjugate after 24 h accounting for 14.9 ± 1.8 % (DFO-*p*-Ph-NCS) and 35.0 ± 1.4 % (DFO*-*p*-Ph-NCS). Even though the stability in human serum seems to be insufficiently low in both cases, the extended system DFO* nevertheless provided improved results compared to its parental structure DFO. Underlining the already mentioned assumption, the free *p*-

isothiocyanatophenyl moiety obviously led to significantly reduced *in vitro* stability of respectively ^{89}Zr-labeled chelators in human serum.

3.4 Antibody coupling and radiolabeling of the resulting immunoconjugates

The novel bifunctional derivatives Hy_3ADA^5-SA and Hy_3ADA^5-*p*-Ph-NCS were coupled to lysine side chains of the model protein bevacizumab via either pH dependent second amidation of the squaric acid monoamide or formation of a stable thiourea bond. The ratio of respectively conjugated chelators per protein (CAR) was determined using mass spectrometric analysis via MALDI-TOF (Fig. S2, Table 1). ^{89}Zr-complexation kinetics were subsequently evaluated using the same conditions as for unbound chelators described in section 3.2. Again, squaramide-functionalized DFO-SA as well as DFO-*p*-Ph-NCS and DFO*-*p*-Ph-NCS served as references being analogously coupled, purified, characterized and radiolabeled (Fig. 5).

Fig. 5

Successful coupling of the corresponding chelator to the antibody could be confirmed for all investigated conjugates providing a shift to higher molecular weights in the MALDI-TOF mass spectrum compared to the non-functionalized protein (Fig. S2). Dividing the mass difference by the mass gain per conjugated chelator moiety respectively led to the calculated CAR values shown in Table 1. Hence, utilization of a tenfold molar excess of the chelator resulted in an average ratio of 2.68 for Hy_3ADA^5-SA-mAb, 1.03 for Hy_3ADA^5-*p*-Ph-NCS-mAb, 3.20 for DFO-SA-mAb, 1.94 for DFO-*p*-Ph-NCS-mAb and 0.87 for DFO*-*p*-Ph-NCS-mAb. Coupling via formation of squaric acid diamides thus generally tended to show a superior efficiency leading to higher numbers of protein-bound chelator moieties compared to the thiourea-based strategy. However, this may also be partly due to the different duration used for conjugation reactions. Furthermore, among all investigated conjugates, there is a trend of the CAR value to increase along with decreasing molecular weight of the bifunctional chelator, which is presumably due to a lower steric demand and therefore higher accessibility. Considering the fact that

either lower or higher molar excesses of the chelator system were used, the herein obtained CAR values of the DFO- and DFO*-functionalized immunoconjugates were comparable to those reported in the literature (DFO-SA: 20 eq., CAR = 3.4–4.5 [25]; DFO-*p*-Ph-NCS: 3 eq., CAR = 0.3–1.5 [15,24,25,53]; DFO*-*p*-Ph-NCS: 3 eq., CAR = 0.6–0.8 [24]).

Table 1

The Hy_3ADA^5-SA- and Hy_3ADA^5-*p*-Ph-NCS-modified immunoconjugates indicated promising ^{89}Zr-labeling results at mild conditions leading to high radiochemical conversions of 82.0 ± 1.1 % and 89.2 ± 0.7 %, respectively after 90 min (Fig. 6, Table S4). Here, the *p*-isothiocyanatophenyl-derivative showed not only a slightly better final result, but also consistently faster labeling kinetics as reflected by 60.7 ± 7.1 % already after 30 min compared to 46.7 ± 5.1 % obtained for the squaramide-analogue after the same duration. Similar to the observed behavior of the stand-alone chelators (3.2) and to the results reported by Chomet *et al*., the additional donor atoms introduced by the squaric acid moiety therefore had no enhancing influence on the complexation properties of the actual chelator at least under the conditions used herein [27].

Fig. 6

Using identical conditions, the linear analogues DFO-SA-mAb and DFO-*p*-Ph-NCS-mAb revealed even better ^{89}Zr-labeling properties providing fast and high yielding complexation of the radiometal. Initially, the squaramide coupled conjugate showed slightly faster labeling kinetics with radiochemical conversions of 60.2 ± 4.4 % after 15 min compared to the formation of [^{89}Zr]Zr-DFO-*p*-Ph-NCS-mAb accounting for 53.9 ± 1.1 %. Nevertheless, the values of both conjugates converged in the further course of the experiment, leading to almost identical results of approx. 95 % after 90 min. As similarly observed in the case of unbound chelators described in section 3.2, the DFO*-functionalized protein provided the highest radiochemical conversion of all investigated antibody conjugates up to 98.8 ± 0.4 % after 90 min.

As expected, all investigated chelator derivatives showed slower labeling kinetics if bound to the antibody compared to their free, unbound version. On the one hand, this may be partly due to divergent effective concentrations of the corresponding complex-forming moiety within the labeling samples. While radiolabeling of the stand-alone chelators was performed using 20 nmol (26.7 µM) each, the actual amounts of their protein-bound analogues in the follow-up experiment accounted for 4.1–11.9 nmol (5.4–15.9 µM), as calculated from the used quantities of the immunoconjugates and corresponding CAR-values. On the other hand, the steric demand of the large biomolecule leads to reduced accessibility of the corresponding chelator presumably representing the main cause for an impaired complexation. [^{89}Zr]Zr-DFO*-*p*-Ph-NCS-mAb showed the most rapid formation as reflected by 70.6 ± 0.3 % protein bound activity already after 15 min. Therefore, the complexation properties of the actual DFO*-chelator are obviously less affected by the biomolecule compared to the other systems.

In summary, the novel Hy_3ADA^5 chelator derivatives indicated slightly slower ^{89}Zr-complexation compared to the DFO and DFO*-analogues, especially if coupled to the antibody (82–89 % versus 95–99 % RCC after 90 min). While the linear DFO contains a variety of freely rotatable C–C bonds, the cyclic and more rigid 1,4-diazepane backbone of Hy_3ADA^5 leads to a more restricted flexibility of the hydroxamate donor groups. The hybrid system therefore provides a certain preorganized coordination geometry, which in turn requires less structural adjustments in the process of radiometal complexation. While formation of the [^{89}Zr]Zr-Hy_3ADA^5-complex should thus be thermodynamically favorable, apparently, it is kinetically more hindered than complexation via DFO. Representing a key property of hybrid chelators, the activation energy of [^{89}Zr]Zr-Hy_3ADA^5 is assumed to be higher than that based on linear systems but significantly lower than that of macrocyclic structures, due to the additional acyclic component. On the one hand, these characteristics ensure high yielding complexation of the radiometal already at room temperature, but may presumably also be responsible for the observed slightly slower labeling kinetics compared to linear DFO derivatives. In the case of antibody conjugates, the differences in radiolabeling efficiency were found to be more pronounced

than those of the unbound chelators. Hence, the accessibility of the Hy_3ADA^5 system seems to be more affected by the additional steric demand of the large biomolecule than that of flexible DFO and DFO*. Since the curves of both [^{89}Zr]Zr-Hy_3ADA^5-SA-mAb and [^{89}Zr]-Hy_3ADA^5-*p*-Ph-NCS-mAb do not seem to have reached a maximum at the end of the labeling experiment, probably even higher yields could be achieved by further extending the incubation time or by using slightly elevated temperatures.

3.5 *In vitro* complex stability of the ^{89}Zr-labeled Hy_3ADA^5- and DFO-functionalized immunoconjugates

Prior to evaluation of their *in vitro* complex stability, the radioimmunoconjugates were purified via second SEC to remove unbound zirconium-89 and small molecule components as well as to exchange the reaction medium to PBS (Fig. S1). All investigated protein-bound complexes, based on both Hy_3ADA^5 and DFO, indicated no significant release of radiometal in either formulation medium or human serum, at least within the 7-day time interval evaluated herein (Fig. 7, Table S5, S6). Starting from an initial radiochemical purity of 92 %, even slightly increased values of 94.2 ± 2.5 % and 94.1 ± 0.3 % protein bound activity could be observed for [^{89}Zr]Zr-Hy_3ADA^5-SA-mAb in PBS and human serum, respectively at the end of measurement. Presumably caused by further complexation, minor release and recomplexation, marginal fluctuations in the range of about 5–6 % occurred in both media throughout the experiment. Investigating the thiourea-coupled analogue [^{89}Zr]Zr-Hy_3ADA^5-*p*-Ph-NCS-mAb, no significant changes in the amount of incorporated activity neither positive nor negative could be observed over the entire period of 7 days in both media. Final values of 95.5 ± 0.1 % (PBS) and 94.4 ± 1.0 % (human serum) intact conjugate, based on an initial purity of 94.6 %, could successfully confirm the high stability of the actual [^{89}Zr]Zr-Hy_3ADA^5 complex already represented by aforementioned results.

The DFO bearing references [^{89}Zr]Zr-DFO-SA-mAb and [^{89}Zr]Zr-DFO-*p*-Ph-NCS-mAb as well as the extended system [^{89}Zr]Zr-DFO*-*p*-Ph-NCS-mAb could be obtained with slightly higher radiochemical

purities of 97–100 % after SEC. Subsequent incubation at 37 °C in PBS and human serum over a period of 7 days nevertheless led to almost identical results representing a constantly stable complexation of the radiometal without exception. In both media, the percentages of protein bound activity remained almost unchanged (difference < 1.5 %) for all three conjugates within the entire period.

At least under the conditions used herein, therefore neither significant advantages nor disadvantages of the different coupling strategies (SA, *p*-Ph-NCS) and actual chelator systems (Hy_3ADA^5, DFO, DFO*) regarding *in vitro* complex stability could be observed, since all investigated conjugates provided excellent results.

Fig. 7

4. Conclusion

In the present study, we introduced the development and *in vitro* evaluation of novel bifunctional ^{89}Zr-chelators based on the well-established hybrid 6-amino-1,4-diazepane backbone in combination with hydroxamic acid bearing sidechains. Both stand-alone and coupled to a model antibody, Hy_3ADA^5 as well as two further derivatives being extended by either a squaramide or *p*-isothiocyanatophenyl moiety indicated fast and high yielding complexation of ^{89}Zr (82–94 % RCC) at mild conditions as well as high *in vitro* complex stability over a period of 7 days (release < 3 %). Utilization of deferoxamine as linear gold standard for complexation of tetravalent zirconium-89 and its extended version DFO* led to even slightly faster radiolabeling and similarly high *in vitro* complex stabilities of the corresponding analogues. A considerable instability of all *p*-isothiocyanatophenyl-functionalized derivatives in human serum only occurred using the chelator systems stand-alone, but not bound to an antibody. Since the frequently reported instability of the [^{89}Zr]Zr-DFO complex appears to be a phenomenon mainly occurring in animal studies, the excellent properties of Hy_3ADA^5 described in this work are to be further investigated and compared in future *in vivo* studies. Nevertheless, this novel chelator represents a promising candidate for fast and stable radiolabeling of monoclonal antibodies with zirconium-89 concerning immuno-PET applications.

List of abbrevations

AAZTA: 1,4-Bis(carboxymethyl)-6-[bis(carboxymethyl)]amino-6-methylperhydro-1,4-diazepine; AAZTA^5: 1,4-Bis(carboxymethyl)-6-[bis(carboxymethyl)]amino-6-[pentanoic-acid]perhydro-1,4-diazepine; Boc: *tert*-Butyloxycarbonyl protecting group; CAR: Chelator-to-antibody ratio; DATA^m: 1,4-Bis(carboxymethyl)-6-[(carboxymethyl)methylamino]-6-methylperhydro-1,4-diazepine; DATA^{5m}: 1,4-Bis(carboxymethyl)-6-[(carboxymethyl)methylamino]-6-[pentanoic-acid]perhydro-1,4-diazepine; DFO: Deferoxamine; DFO*: Deferoxamine*; DIPEA: *N*,*N*-Diisopropylethylamine; DMF: Dimethylformamide; DMSO: Dimethyl sulfoxide; ESI: Electrospray ionization; Et_3N: Triethylamine; EtOH: Ethanol; HATU: 1-[Bis(dimethylamino)methylene]-1*H*-1,2,3-triazolo[4,5-b]pyridinium 3-oxide hexafluorophosphate; HBTU: 2-(1*H*-Benzotriazol-1-yl)-1,1,3,3-tetramethyluronium hexafluorophosphate; HEPES: 4-(2-Hydroxyethyl)-1-piperazineethanesulfonic acid; HOBt: Hydroxybenzotriazole; HOPO: Hydroxypyridinone; HPLC: High-performance liquid chromatography; HS: Human serum; LC: Liquid chromatography; mAb: Monoclonal antibody; MALDI: Matrix-assisted laser desorption/ionization; MeCN: Acetonitrile; MeOH: Methanol; MS: Mass spectrometry; n.c.a.: No-carrier-added; NMR: Nuclear magnetic resonance; PBS: Phosphate buffered saline; PET: Positron emission tomography; RCC: Radiochemical conversion; RT: Room temperature; SA: Squaric acid; SD: Standard deviation; SEC: Size exclusion chromatography; TAM: Terephthalamide; TFA: Trifluoroacetic acid; THF: Tetrahydrofuran; TLC: Thin layer chromatography; TOF: Time-of-flight; VEGF: Vascular endothelial growth factor

Ethical approval: Not applicable.

Competing interests: TLM and GG are co-inventors on pending patent applications describing DFO* and its derivatives. These patent applications are owned by the University of Zurich and the University

of Basel. The patent owners have granted an exclusive license to the company ABX Advanced Biochemicals Compounds. The inventors are unrelated to this company.

Funding: This work was funded in part by the Swiss National Science Foundation (grant Nr. SNSF 205321_157216 to GG and TLM).

Author´s contribution: BK planned and conceived the present study and wrote the manuscript. BK and DL were in charge for organic synthesis. BK performed radiochemical synthesis and evaluation. TLM and GG contributed for the interpretation of the results. FR supervised the whole part of the study. All authors read and approved the manuscript.

Acknowledgements: The authors would like to thank Riem Attariya for determination of protein concentrations and Dr. Elena Berger-Nicoletti for MALDI-TOF measurements. We are also very grateful to the Collaborative Research Center SFB 1066 of the German Research Foundation (DFG) for its support.

Additional files

Supporting Information

Fig. S1.

Fig. S2.

References

[1] Zhang Y, Hong H, Cai W. PET tracers based on zirconium-89. Curr Radiopharm 2011;4:131–9.

[2] Wei W, Rosenkrans ZT, Liu J, Huang G, Luo QY, Cai W. ImmunoPET: concept, design, and applications. Chem Rev 2020;120:3787–851.

[3] Goldenberg DM, Sharkey RM. Novel radiolabeled antibody conjugates. Oncogene 2007;26:3734–44.

[4] Boswell CA, Brechbiel MW. Development of radioimmunotherapeutic and diagnostic antibodies: an inside-out view. Nucl Med Biol 2007;34:757–78.

[5] Moek KL, Giesen D, Kok IC, de Groot DJA, Jalving M, Fehrmann RSN, et al. Theranostics using antibodies and antibody-related therapeutics. J Nucl Med 2017;58:83S-90S.

[6] Heskamp S, Raavé R, Boerman O, Rijpkema M, Goncalves V, Denat F. ^{89}Zr-Immuno-positron emission tomography in oncology: state-of-the-art ^{89}Zr radiochemistry. Bioconjug Chem 2017;28:2211–23.

[7] Bhatt NB, Pandya DN, Wadas TJ. Recent advances in zirconium-89 chelator development. Molecules 2018;23.

[8] van de Watering FCJJ, Rijpkema M, Perk L, Brinkmann U, Oyen WJGG, Boerman OC. Zirconium-89 labeled antibodies: a new tool for molecular imaging in cancer patients. Biomed Res Int 2014;2014:1–13.

[9] Deri MA, Zeglis BM, Francesconi LC, Lewis JS. PET imaging with ^{89}Zr: from radiochemistry to the clinic. Nucl Med Biol 2013;40:3–14.

[10] Wooten A, Madrid E, Schweitzer G, Lawrence L, Mebrahtu E, Lewis B, et al. Routine production of ^{89}Zr using an automated module. Appl Sci 2013;3:593–613.

[11] Disselhorst JA, Brom M, Laverman P, Slump CH, Boerman OC, Oyen WJGG, et al. Image-quality assessment for several positron emitters using the NEMA NU 4-2008 standards in the siemens inveon small-animal PET scanner. J Nucl Med 2010;51:610–7.

[12] Bé M-M, Chisté V, Dulieu C, Kellett MA, Mougeot X, Arinc A, et al. Table of radionuclides. vol. 8. Bureau International Des Poids Et Mesures; 2016.

[13] Dilworth JR, Pascu SI. The chemistry of PET imaging with zirconium-89. Chem Soc Rev 2018;47:2554–71.

[14] Bailey DL, Townsend DW, Valk PE, Maisey MN, editors. Positron emission tomography. London: Springer-Verlag; 2005.

[15] Perk LR, Vosjan MJWD, Visser GWM, Budde M, Jurek P, Kiefer GE, et al. P-Isothiocyanatobenzyl-desferrioxamine: A new bifunctional chelate for facile radiolabeling of monoclonal antibodies with zirconium-89 for immuno-PET imaging. Eur J Nucl Med Mol Imaging 2010;37:250–9.

[16] Toporivska Y, Gumienna-Kontecka E. The solution thermodynamic stability of desferrioxamine B (DFO) with Zr(IV). J Inorg Biochem 2019;198:110753.

[17] Holland JP, Divilov V, Bander NH, Smith-Jones PM, Larson SM, Lewis JS. ^{89}Zr-DFO-J591 for immunoPET of prostate-specific membrane antigen expression in vivo. J Nucl Med 2010;51:1293–300.

[18] Guérard F, Lee YS, Tripier R, Szajek LP, Deschamps JR, Brechbiel MW. Investigation of Zr(IV) and ^{89}Zr(IV) complexation with hydroxamates: Progress towards designing a better chelator than desferrioxamine B for immuno-PET imaging. Chem Commun 2013;49:1002–4.

[19] Abou DS, Ku T, Smith-Jones PM. In vivo biodistribution and accumulation of ^{89}Zr in mice. Nucl Med Biol 2011;38:675–81.

[20] Heskamp S, Van Laarhoven HWM, Molkenboer-Kuenen JDM, Franssen GM, Versleijen-Jonkers YMH, Oyen WJG, et al. ImmunoSPECT and immunoPET of IGF-1R expression with the radiolabeled antibody R1507 in a triple-negative breast cancer model. J Nucl Med 2010;51:1565–72.

[21] Perk LR, Visser GWM, Vosjan MJWD, Stigter-Van Walsum M, Tijink BM, Leemans CR, et al. ^{89}Zr as a PET surrogate radioisotope for scouting biodistribution of the therapeutic radiometals ^{90}Y and ^{177}Lu in tumor-bearing nude mice after coupling to the internalizing antibody cetuximab. J Nucl Med 2005;46:1898–906.

[22] Laverman P, Van Der Geest T, Terry SYA, Gerrits D, Walgreen B, Helsen MM, et al. Immuno-PET and immuno-SPECT of rheumatoid arthritis with radiolabeled anti-fibroblast activation protein antibody correlates with severity of arthritis. J Nucl Med 2015;56:778–83.

[23] Patra M, Bauman A, Mari C, Fischer CA, Häussinger D, Gasser G, et al. An octadentate bifunctional chelating agent for the development of stable zirconium-89 based molecular imaging probes. Chem Commun 2014;50:11523–5.

[24] Vugts DJ, Klaver C, Sewing C, Poot AJ, Adamzek K, Huegli S, et al. Comparison of the

octadentate bifunctional chelator DFO*-pPhe-NCS and the clinically used hexadentate bifunctional chelator DFO-pPhe-NCS for ^{89}Zr-immuno-PET. Eur J Nucl Med Mol Imaging 2017;44:286–95.

[25] Rudd SE, Roselt P, Cullinane C, Hicks RJ, Donnelly PS. A desferrioxamine B squaramide ester for the incorporation of zirconium-89 into antibodies. Chem Commun 2016;52:11889–92.

[26] Berg E, Gill H, Marik J, Ogasawara A, Williams S, van Dongen G, et al. Total-body PET and highly stable chelators together enable meaningful ^{89}Zr-antibody PET studies up to 30 days after injection. J Nucl Med 2020;61:453–60.

[27] Chomet M, Schreurs M, Bolijn MJ, Verlaan M, Beaino W, Brown K, et al. Head-to-head comparison of DFO* and DFO chelators: selection of the best candidate for clinical ^{89}Zr-immuno-PET. Eur J Nucl Med Mol Imaging 2021;48:694–707.

[28] Boros E, Holland JP, Kenton N, Rotile N, Caravan P. Macrocycle-based hydroxamate ligands for complexation and immunoconjugation of ^{89}Zirconium for Positron Emission Tomography (PET) imaging. Chempluschem 2016;81:274–81. https://doi.org/10.1002/cplu.201600003.

[29] Raavé R, Sandker G, Adumeau P, Jacobsen CB, Mangin F, Meyer M, et al. Direct comparison of the in vitro and in vivo stability of DFO, DFO* and DFOcyclo* for ^{89}Zr-immunoPET. Eur J Nucl Med Mol Imaging 2019;46:1966–77.

[30] Zhai C, Summer D, Rangger C, Franssen GM, Laverman P, Haas H, et al. Novel bifunctional cyclic chelator for ^{89}Zr labeling–radiolabeling and targeting properties of RGD conjugates. Mol Pharm 2015;12:2142–50.

[31] Briand M, Aulsebrook ML, Mindt TL, Gasser G. A solid phase-assisted approach for the facile synthesis of a highly water-soluble zirconium-89 chelator for radiopharmaceutical development. Dalt Trans 2017;46:16387–9.

[32] Brandt M, Cowell J, Aulsebrook ML, Gasser G, Mindt TL. Radiolabelling of the octadentate chelators DFO* and oxoDFO* with zirconium-89 and gallium-68. JBIC J Biol Inorg Chem 2020;25:789–96.

[33] Deri MA, Ponnala S, Zeglis BM, Pohl G, Dannenberg JJ, Lewis JS, et al. Alternative chelator for ^{89}Zr radiopharmaceuticals: radiolabeling and evaluation of 3,4,3-(LI-1,2-HOPO). J Med Chem 2014;57:4849–60.

[34] Deri MA, Ponnala S, Kozlowski P, Burton-Pye BP, Cicek HT, Hu C, et al. P-SCN-Bn-HOPO: a superior bifunctional chelator for ^{89}Zr immunoPET. Bioconjug Chem 2015;26:2579–91.

[35] Tinianow JN, Pandya DN, Pailloux SL, Ogasawara A, Vanderbilt AN, Gill HS, et al. Evaluation of a 3-hydroxypyridin-2-one (2,3-HOPO) based macrocyclic chelator for $^{89}Zr^{4+}$ and its use for ImmunoPET imaging of HER2 positive model of ovarian carcinoma in mice. Theranostics 2016;6:511–21.

[36] Pandya DN, Pailloux S, Tatum D, Magda D, Wadas TJ. Di-macrocyclic terephthalamide ligands as chelators for the PET radionuclide zirconium-89. Chem Commun 2015;51:2301–3.

[37] Pfister J, Summer D, Rangger C, Petrik M, von Guggenberg E, Minazzi P, et al. Influence of a novel, versatile bifunctional chelator on theranostic properties of a minigastrin analogue. EJNMMI Res 2015;5:74.

[38] Baranyai Z, Uggeri F, Giovenzana GB, Bényei A, Brücher E, Aime S. Equilibrium and kinetic properties of the lanthanoids(III) and various divalent metal complexes of the heptadentate ligand AAZTA. Chem - A Eur J 2009;15:1696–705.

[39] Seemann J, Waldron B, Parker D, Roesch F. DATATOC: a novel conjugate for kit-type ^{68}Ga labelling of TOC at ambient temperature. EJNMMI Radiopharm Chem 2017;1:4.

[40] Sinnes J-P, Nagel J, Waldron BP, Maina T, Nock BA, Bergmann RK, et al. Instant kit preparation of ^{68}Ga-radiopharmaceuticals via the hybrid chelator DATA: clinical translation of [^{68}Ga]Ga-DATA-TOC. EJNMMI Res 2019;9:48.

[41] Farkas E, Nagel J, Waldron BP, Parker D, Tóth I, Brücher E, et al. Equilibrium, kinetic and structural properties of gallium(III) and some divalent metal complexes formed with the new $DATA^{m}$ and $DATA^{5m}$ ligands. Chem - A Eur J 2017;23:10358–71.

[42] Nagy G, Szikra DDD, Trencsényi G, Fekete A, Garai I, Giani AM, et al. AAZTA: an ideal chelating agent for the development of ^{44}Sc PET imaging agents. Angew Chemie - Int Ed 2017;56:2118–22.

[43] Sinnes J, Nagel J, Rösch F. $AAZTA^{5}$/$AAZTA^{5}$-TOC: synthesis and radiochemical evaluation with ^{68}Ga, ^{44}Sc and ^{177}Lu. EJNMMI Radiopharm Chem 2019;4:18.

[44] Greifenstein L, Grus T, Nagel J, Sinnes JP, Rösch F. Synthesis and labeling of a squaric acid containing PSMA-inhibitor coupled to $AAZTA^{5}$ for versatile labeling with ^{44}Sc, ^{64}Cu, ^{68}Ga and ^{177}Lu. Appl Radiat Isot 2020;156:108867.

[45] Greifenstein L, Späth D, Sinnes JP, Grus T, Rösch F. Mild and efficient ^{64}Cu labeling of perhydro-1,4-diazepine derivatives for potential use with large peptides, proteins and antibodies. Radiochim Acta 2020;108:555–63.

[46] Seemann J, Waldron BP, Roesch F, Parker D. Approaching ´kit-type´ labelling with ^{68}Ga: the DATA chelators. ChemMedChem 2015;10:1019–26.

[47] Waldron BP, Parker D, Burchardt C, Yufit DS, Zimny M, Roesch F. Structure and stability of hexadentate complexes of ligands based on AAZTA for efficient PET labelling with gallium-68. Chem Commun 2013;49:579–81.

[48] Parker D, Waldron BP. Conformational analysis and synthetic approaches to polydentate perhydro-diazepine ligands for the complexation of gallium(iii). Org Biomol Chem 2013;11:2827.

[49] Parker D, Waldron BP, Yufit DS. Crystallographic and solution NMR structural analyses of four hexacoordinated gallium(iii) complexes based on ligands derived from 6-amino-perhydro-1,4-diazepine. Dalt Trans 2013;42:8001.

[50] Wurm FR, Klok HA. Be squared: expanding the horizon of squaric acid-mediated conjugations. Chem Soc Rev 2013;42:8220–36.

[51] Tietze LF, Arlt M, Beller M, Glüsenkamp K, Jähde E, Rajewsky MF, et al. Squaric acid diethyl ester: a new coupling reagent for the formation of drug biopolymer conjugates. synthesis of squaric acid ester amides and diamides. Chem Ber 1991;124:1215–21.

[52] Olshvang E, Szebesczyk A, Kozłowski H, Hadar Y, Gumienna-Kontecka E, Shanzer A. Biomimetic ferrichrome: structural motifs for switching between narrow- and broad-spectrum activities in P. putida and E. coli. Dalt Trans 2015;44:20850–8.

[53] Vosjan MJWD, Perk LR, Visser GWM, Budde M, Jurek P, Kiefer GE, et al. Conjugation and radiolabeling of monoclonal antibodies with zirconium-89 for PET imaging using the bifunctional chelate p-isothiocyanatobenzyl-desferrioxamine. Nat Protoc 2010;5:739–43.

[54] Nakamura T, Abe-Kanoh N, Nakamura Y. Physiological relevance of covalent protein modification by dietary isothiocyanates. J Clin Biochem Nutr 2018;62:11–9.

Scheme Captions

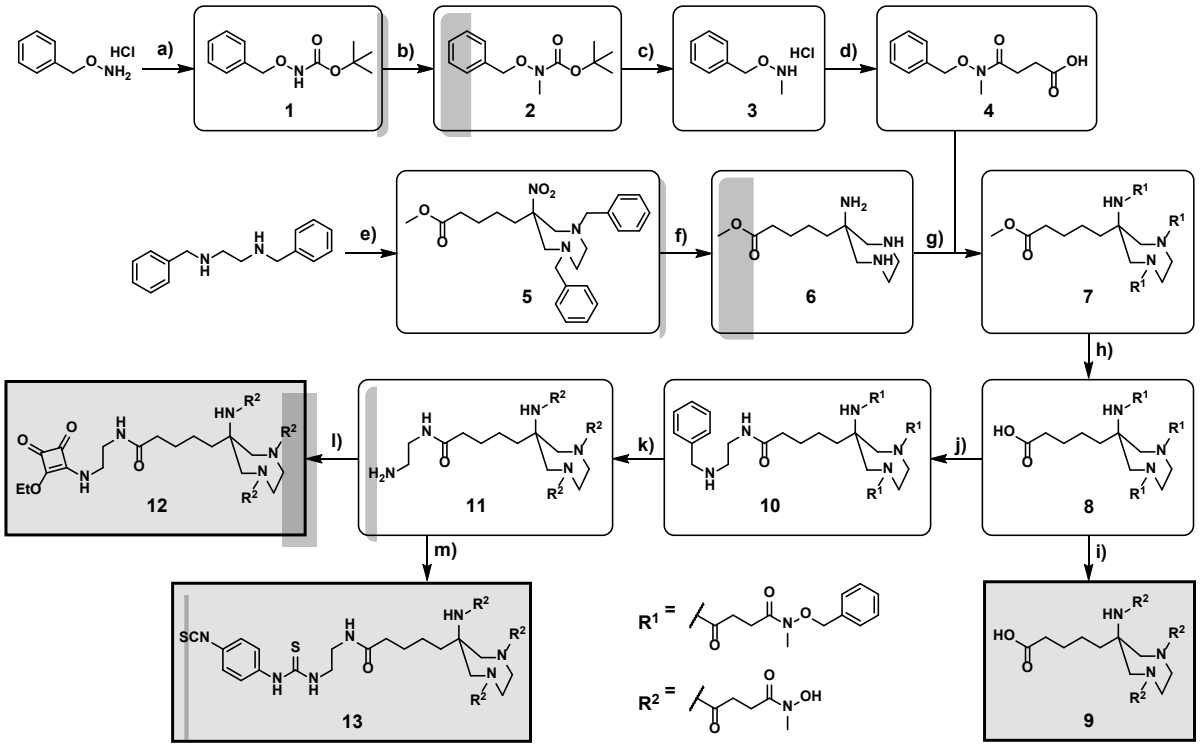

Scheme 1. Schematic overview of the synthesis of Hy_3ADA^5, Hy_3ADA^5-SA and Hy_3ADA^5-*p*-Ph-NCS: (a) di-*tert*-butyl dicarbonate, Et_3N, THF/H_2O (1:1), 97 %; (b) CH_3I, NaH, DMF, 95 %; (c) 4 M HCl in 1,4-dioxane, 100 %; (d) succinic anhydride, 1,4-dioxane, K_2CO_3, 94 %; (e) 2-nitrocyclohexanone, Amberlyst® A21, paraformaldehyde, MeOH, 85 %; (f) $Pd(OH)_2$/C, H_2, MeOH; (g) DIPEA, HATU, DMF, 51 %; (h) 1 M LiOH, 1,4-dioxane/H_2O (2:1), 78 %; (i) Pd/C, H_2, MeOH, 26 %; (j) *N*-benzylethylenediamine, HBTU, HOBt, DIPEA, MeCN, 92 %; (k) Pd/C, H_2, MeOH, 93 %; (l) 3,4-diethoxycyclobut-3-ene-1,2-dione, phosphate-buffer pH 7, 35 %; (m) 1,4-phenylene diisocyanate, isopropanol/water (4:1), chloroform, Et_3N, 28 %.

Figure Captions

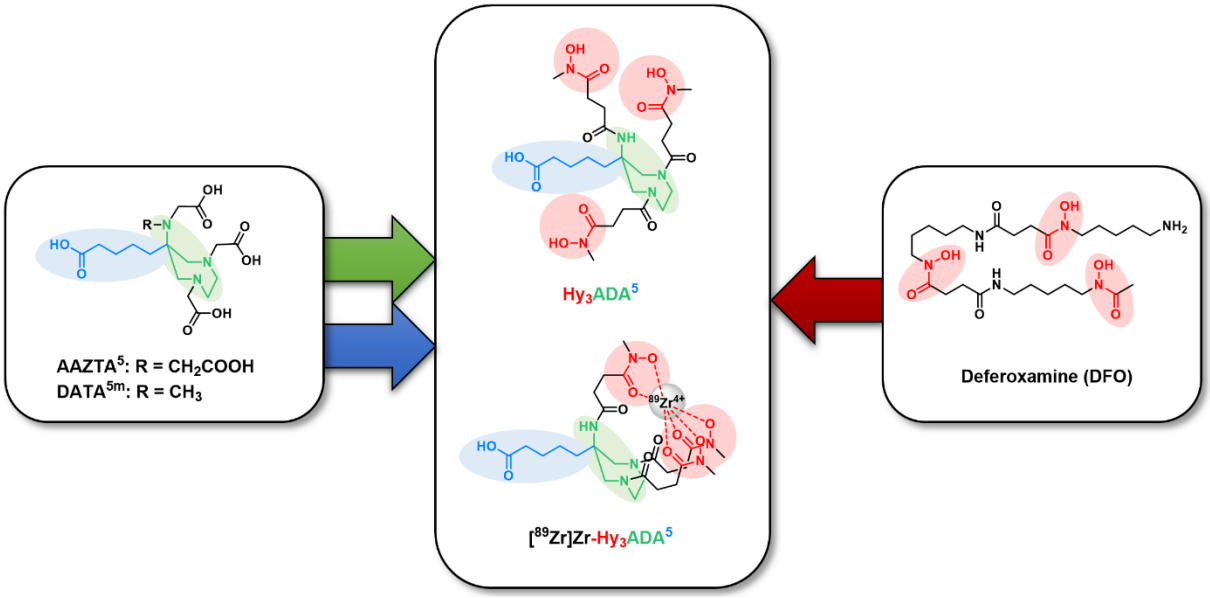

Fig. 1. Schematic overview illustrating the design concept of the new bifunctional ^{89}Zr-chelator Hy_3ADA^5 consisting of a 6-amino-1,4-diazepane backbone (green), a pentanoic acid linker (blue) and three hydroxamate bearing sidechains (red), $AAZTA^5$/$DATA^{5m}$ and deferoxamine served as guiding structures.

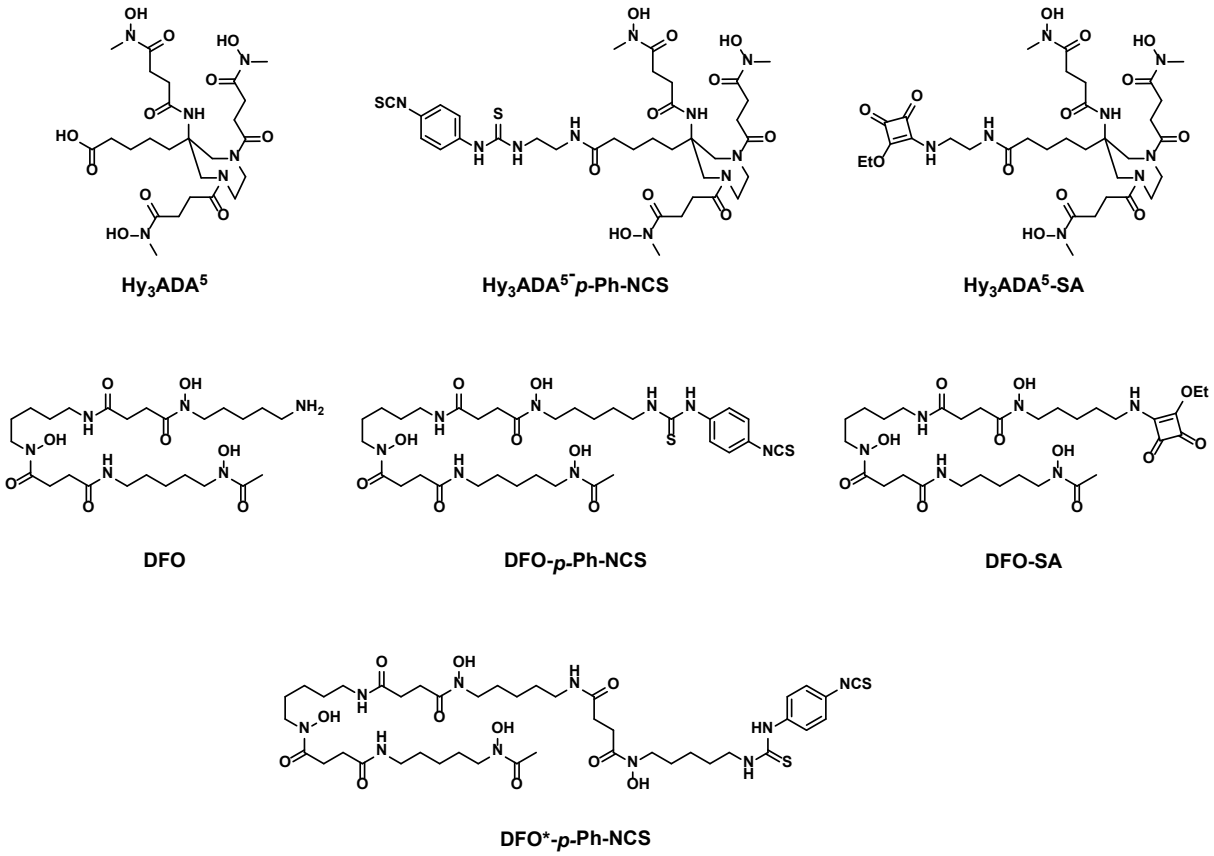

Fig. 2. Overview showing the structures of the novel bifunctional chelators Hy_3ADA^5, Hy_3ADA^5-SA, Hy_3ADA^5-*p*-Ph-NCS as well as of corresponding deferoxamine derivatives DFO, DFO-SA, DFO-*p*-Ph-NCS and DFO*-*p*-Ph-NCS that served as reference systems.

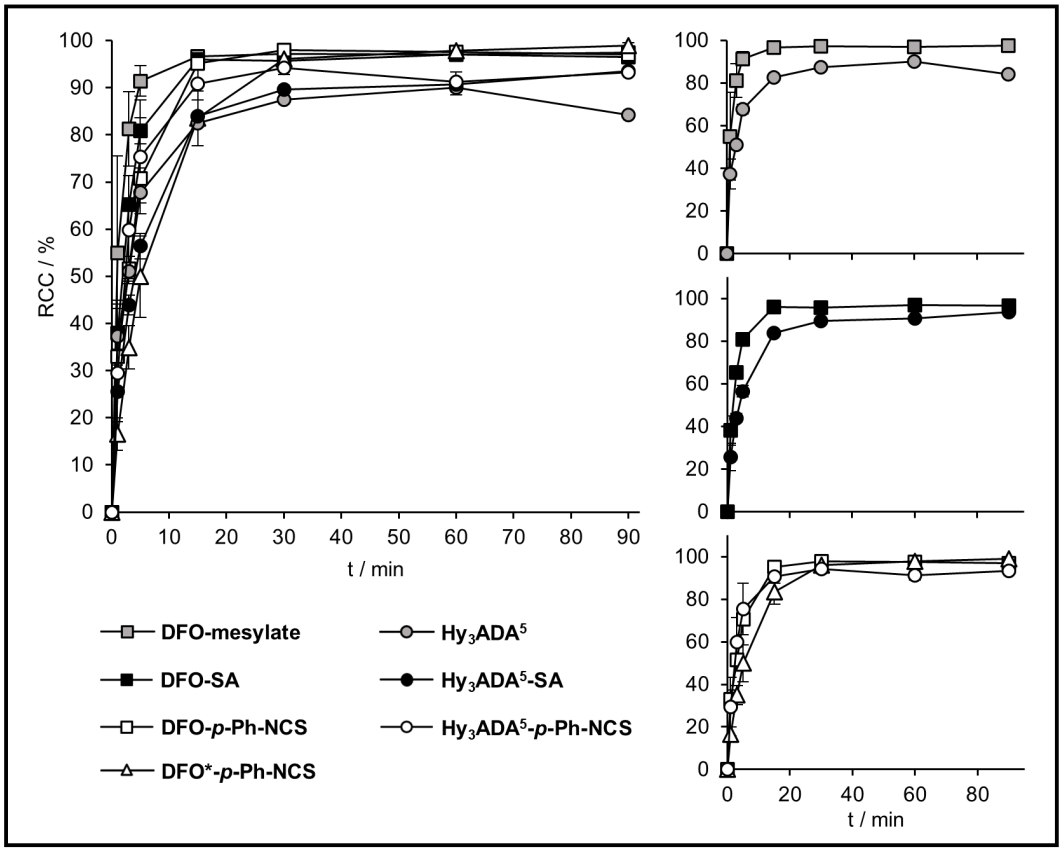

Fig. 3. Radiolabeling efficiency of [^{89}Zr]Zr-Hy_3ADA^5, [^{89}Zr]Zr-Hy_3ADA^5-SA, [^{89}Zr]Zr-Hy_3ADA^5-*p*-Ph-NCS, [^{89}Zr]Zr-DFO, [^{89}Zr]Zr-DFO-SA, [^{89}Zr]Zr-DFO-*p*-Ph-NCS and [^{89}Zr]Zr-DFO*-*p*-Ph-NCS at room temperature using 20 nmol of the respective chelator and 10–12 MBq zirconium-89 in HEPES-buffer (pH 7), values displayed as mean ± SD (*n* = 3).

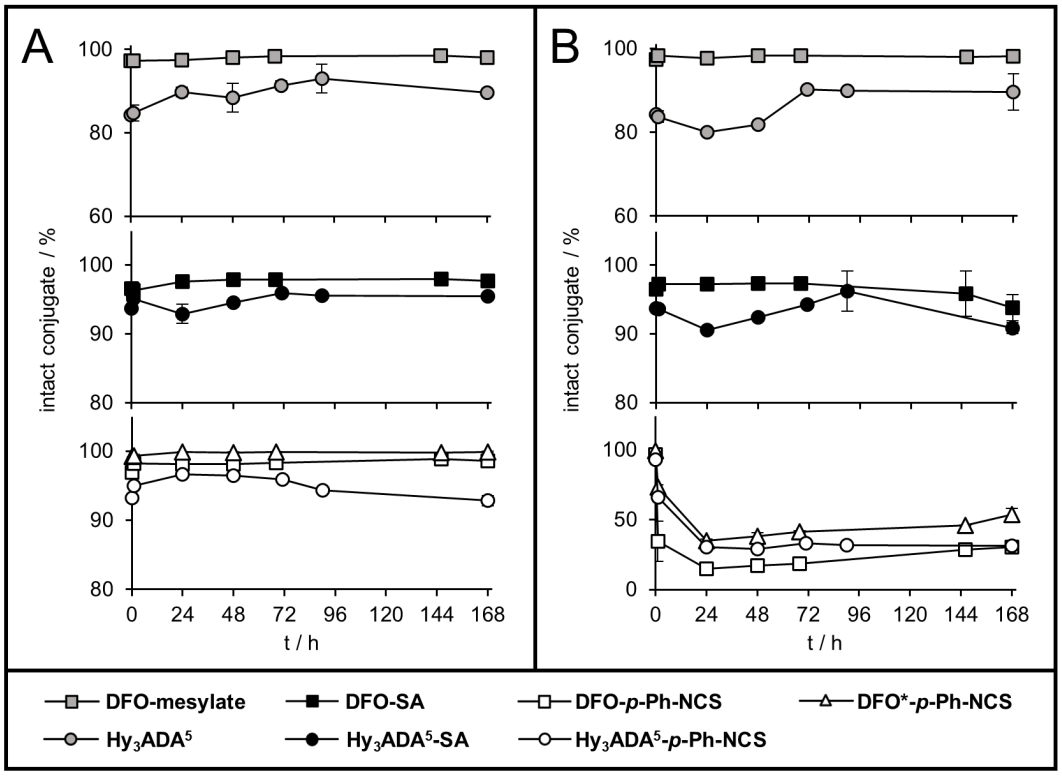

Fig. 4. *In vitro* complex stability of the ^{89}Zr-labeled Hy_3ADA^5- and DFO derivatives in PBS (A) and human serum (B) at 37 °C within 7 d: measured percentages of incorporated activity (radio-TLC) as a function of time starting from radiochemical purity at the end of labeling experiment, values displayed as mean ± SD (*n* = 3).

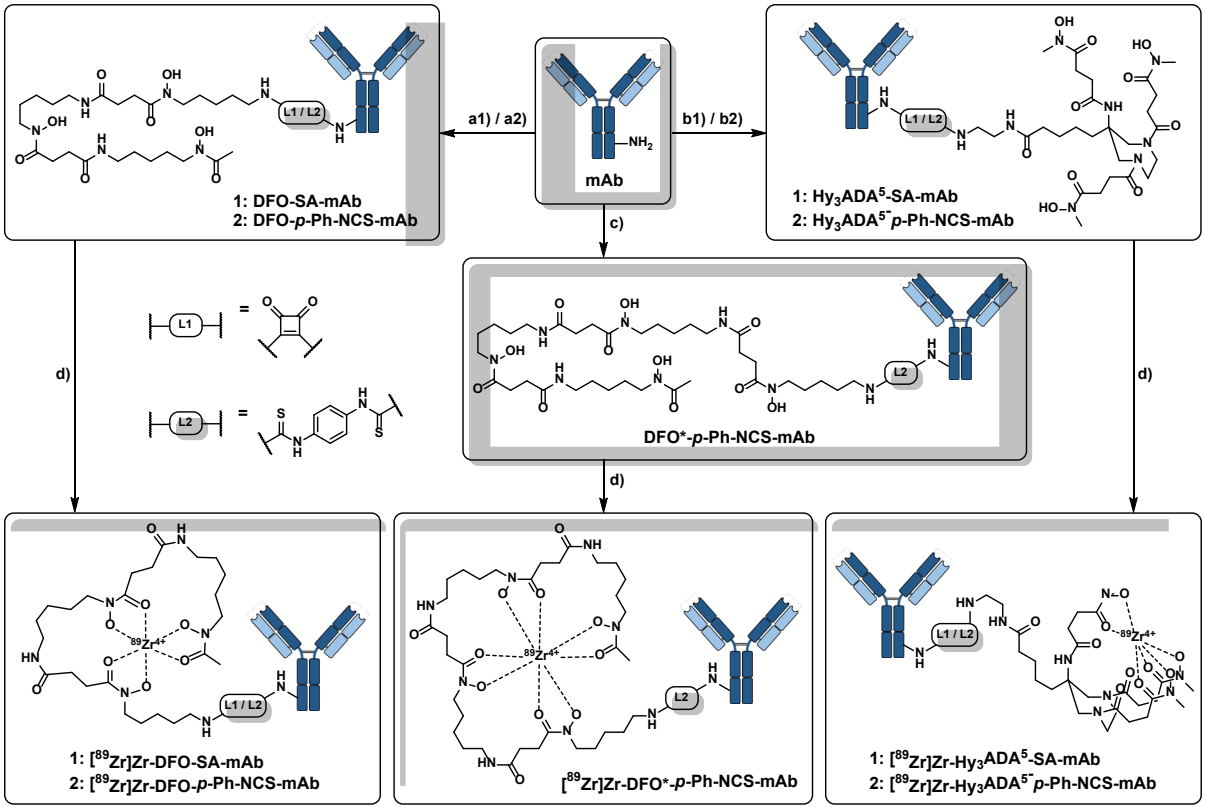

Fig. 5. Synthesis and ^{89}Zr-labeling of the Hy_3ADA^5-, DFO- and DFO*-functionalized antibody conjugates: (a1) 10 eq. DFO-SA, phosphate-buffer pH 9; (a2) 10 eq. DFO-*p*-Ph-NCS, PBS pH 9; (b1) 10 eq. Hy_3ADA^5-SA, phosphate-buffer pH 9; (b2) 10 eq. Hy_3ADA^5-*p*-Ph-NCS, PBS pH 9; (c) 10 eq. DFO*-*p*-Ph-NCS, PBS pH 9; (d) [^{89}Zr]Zr-oxalate, HEPES-buffer pH 7, room temperature.

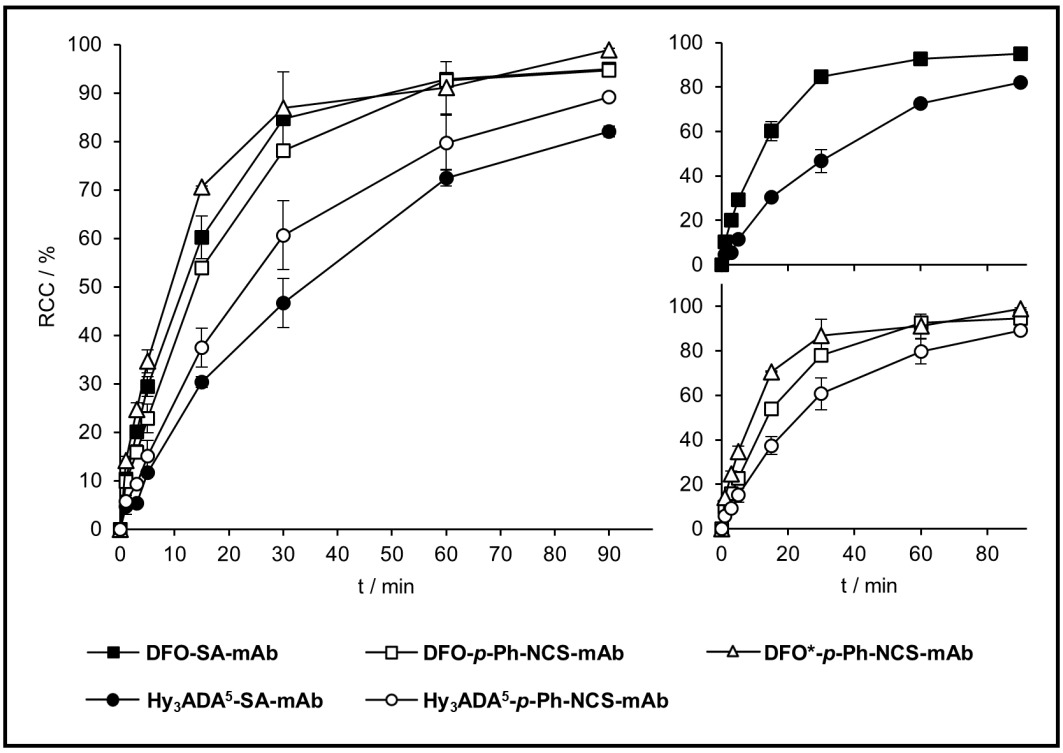

Fig. 6. Radiolabeling efficiency of [^{89}Zr]Zr-Hy$_3$ADA^5-SA-mAb, [^{89}Zr]Zr-Hy$_3$ADA^5-*p*-Ph-NCS-mAb, [^{89}Zr]Zr-DFO-SA-mAb, [^{89}Zr]Zr-DFO-*p*-Ph-NCS-mAb and [^{89}Zr]Zr-DFO*-*p*-Ph-NCS-mAb at room temperature using 472–731 µg of immunoconjugate and 10–12 MBq zirconium-89 in HEPES-buffer (pH 7), values displayed as mean ± SD (*n* = 3).

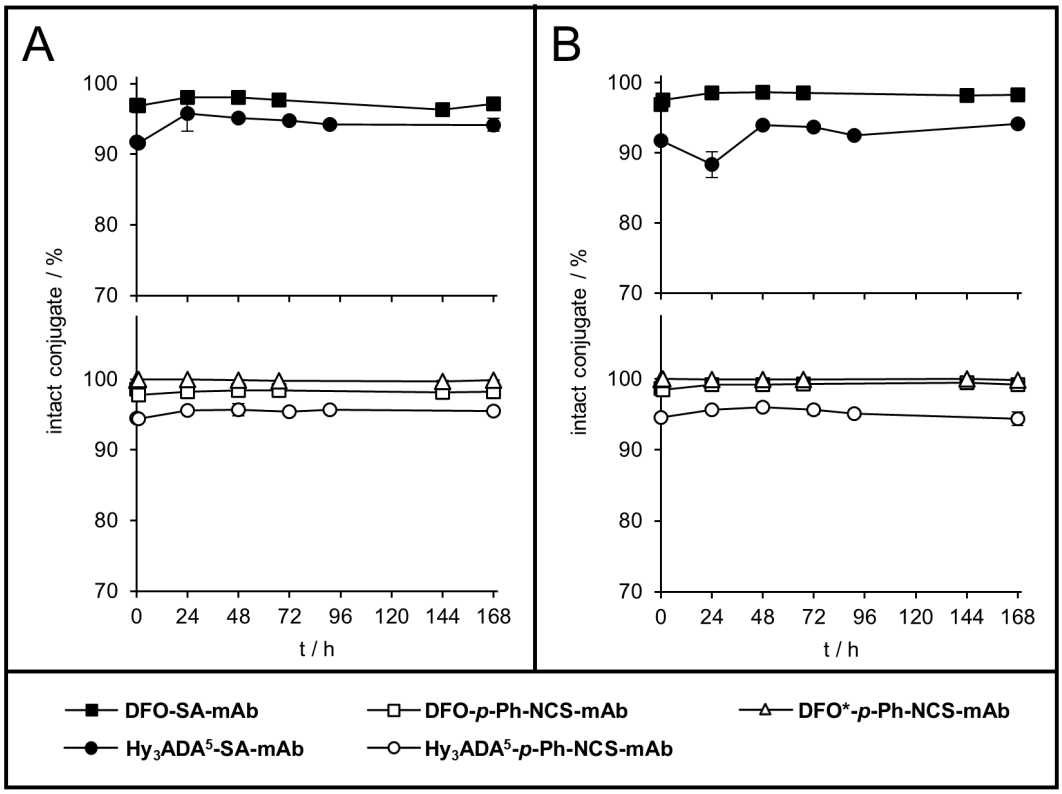

Fig. 7. *In vitro* complex stability of the ^{89}Zr-labeled Hy_3ADA^5- and DFO-functionalized immunoconjugates in PBS (A) and human serum (B) at 37 °C within 7 d: measured percentages of incorporated activity (radio-TLC) as a function of time starting from radiochemical purity after SEC, values displayed as mean ± SD (*n* = 3).

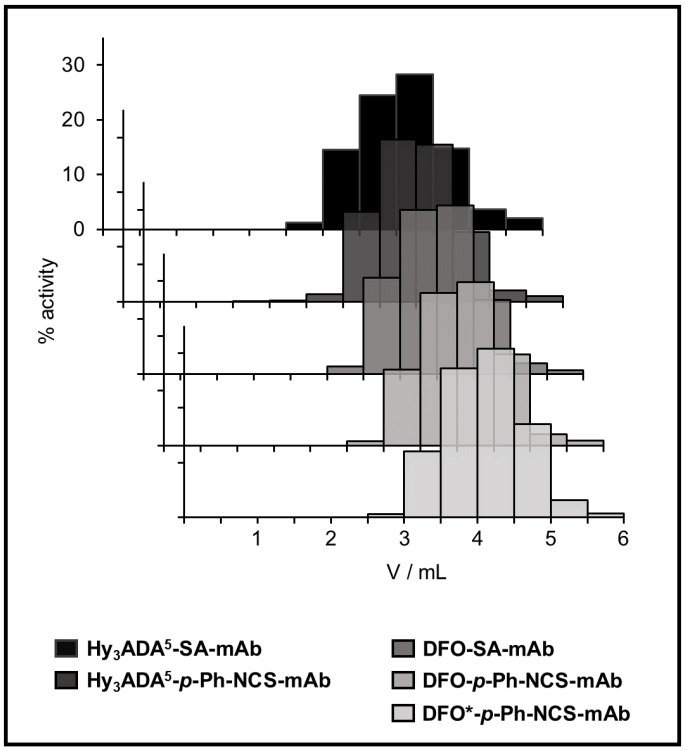

Fig. S1. Purification of the Hy_3ADA^5- and DFO-functionalized immunoconjugates via size exclusion chromatography: elugrams displaying the distribution of radioactivity in consecutive fractions of 0.5 mL PBS.

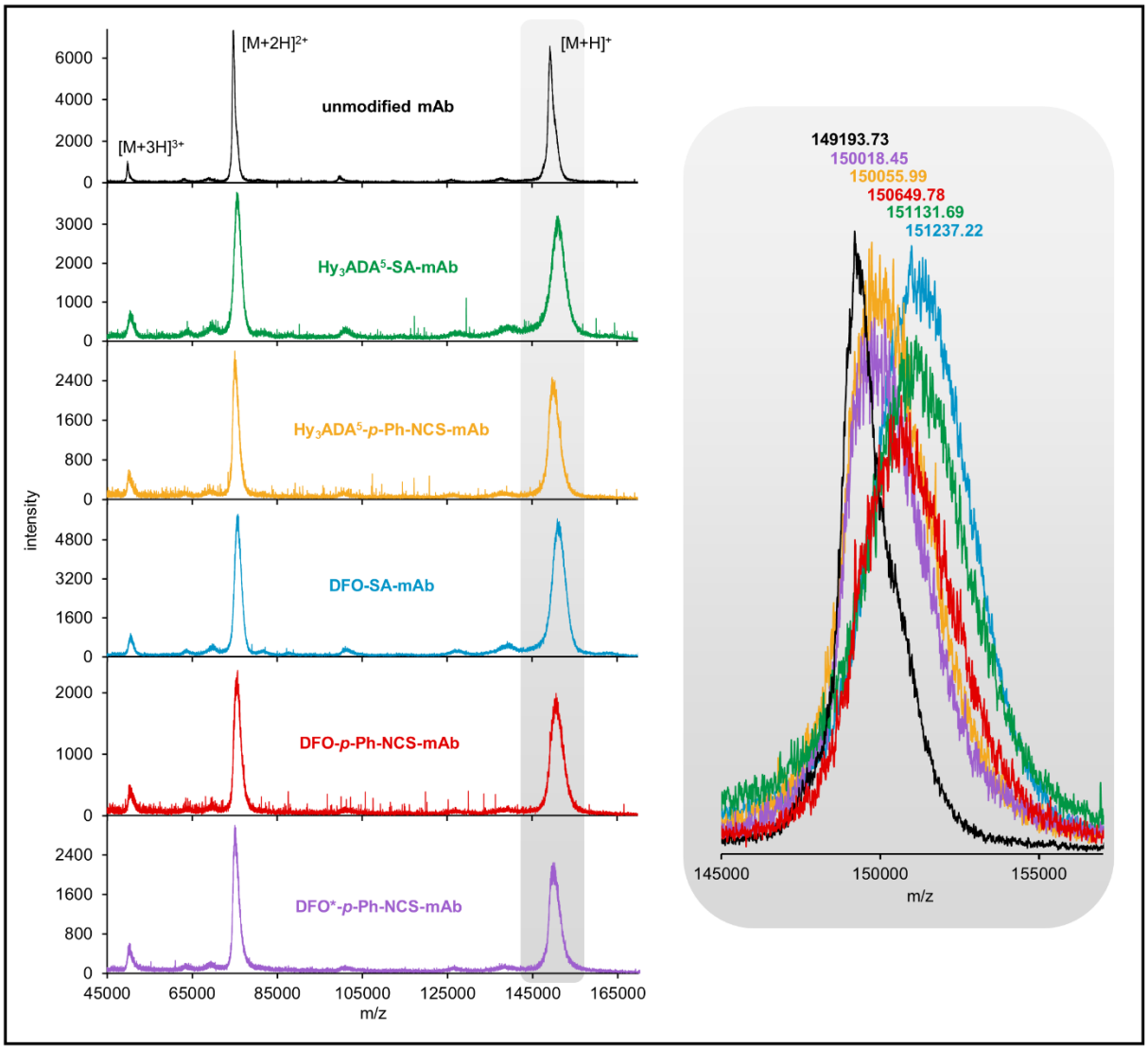

Fig. S2. MALDI-TOF mass spectra of the unmodified antibody and of the Hy_3ADA^5-, DFO- and DFO*-functionalized immunoconjugates.

Tables

Table 1. Measured average molecular weights, mass shifts referenced to the unmodified antibody and calculated chelator-to-antibody ratios (CAR) of the Hy_3ADA^5-, DFO- and DFO*-functionalized immunoconjugates.

Antibody / conjugate	Measured average mass (Da)	Mass shift (Da)	Mass gain per chelator (Da)	CAR
unmodified mAb	149,192.73	–	–	–
Hy_3ADA^5-SA-mAb	151,130.69	1,937.96	722.32	2.68
Hy_3ADA^5-*p*-Ph-NCS-mAb	150,054.99	862.26	836.33	1.03
DFO-SA-mAb	151,236.22	2,043.49	638.33	3.20
DFO-*p*-Ph-NCS-mAb	150,648.78	1,456.05	752.33	1.94
DFO*-*p*-Ph-NCS-mAb	150,017.45	824.72	952.45	0.87